



# Bed and width oscillations form coherent patterns in a partially confined, regulated gravel–cobble-bedded river adjusting to anthropogenic disturbances

Rocko A. Brown<sup>1,2</sup> and Gregory B. Pasternack<sup>1</sup>

<sup>1</sup>University of California, Davis, 1 Shields Avenue, Davis, CA, USA

<sup>2</sup>Environmental Science Associates, 2600 Capitol Avenue, Suite 200, Sacramento, CA, USA

*Correspondence to:* Rocko A. Brown (rokbrown@ucdavis.edu)

Received: 5 December 2015 – Published in Earth Surf. Dynam. Discuss.: 5 February 2016

Revised: 15 November 2016 – Accepted: 6 December 2016 – Published: 11 January 2017

**Abstract.** Understanding the spatial organization of river systems in light of natural and anthropogenic change is extremely important because it can provide information to assess, manage, and restore them to ameliorate worldwide freshwater fauna declines. For gravel- and cobble-bedded alluvial rivers studies spanning analytical, empirical and numerical domains suggest that at channel-forming flows there is a tendency towards covarying bankfull bed and width undulations amongst morphologic units such as pools and riffles, whereby relatively wide areas have relatively higher minimum bed elevations and relatively narrow areas have relatively lower minimum bed elevations. The goal of this study was to determine whether minimum bed elevation and flow-dependent channel top width are organized in a partially confined, incising gravel–cobble bed river with multiple spatial scales of anthropogenic and natural landform heterogeneity across a range of discharges. A key result is that the test river exhibited covarying oscillations of minimum bed elevation and channel top width across all flows analyzed. These covarying oscillations were found to be quasiperiodic at channel-forming flows, scaling with the length scales of bars, pools and riffles. Thus, it appears that alluvial rivers organize their topography to have quasiperiodic, shallow and wide or narrow and deep cross section geometry, even despite ongoing, centennial-scale incision. Presumably these covarying oscillations are linked to hydrogeomorphic mechanisms associated with alluvial river channel maintenance. The biggest conclusion from this study is that alluvial rivers are defined more so by variability in topography and flow than mean conditions. Broader impacts of this study are that the methods provide a framework for characterizing longitudinal and flow-dependent variability in rivers for assessing geomorphic structure and aquatic habitat in space, and if repeated, through time.

## 1 Introduction

Understanding the spatial organization of river systems in light of natural and anthropogenic change is extremely important because it can provide information to assess, manage and restore them to ameliorate worldwide freshwater fauna declines (Frissell et al., 1986; Richter et al., 1997). Alluvial rivers found in transitional upland–lowland environments with slopes  $< 0.02$  and median diameter bed sediments ranging from 8 to 256 mm can exhibit scale-dependent organization of their bed sediments (Milne, 1982), bed elevation profile (Madej, 2001), cross section geometry (Rayberg

and Neave, 2008), and morphological units (Keller and Melhorn, 1978; Thomson et al., 2001). For these rivers a plethora of studies spanning analytical, empirical, and numerical domains suggest that at channel-forming flows, there is a tendency towards covarying bankfull bed and width undulations amongst morphologic units such as pools and riffles (Brown et al., 2016). That is, relatively wide areas have higher relative bed elevations and relatively narrow areas have lower relative bed elevations. While covarying bed and width undulations have been evaluated in field studies using cross section data (Richards, 1976a, b), in models of sediment transport and water flow (Repetto and Tubino, 2001), flume studies

(Nelson et al., 2015), and in theoretical treatments (Huang et al., 2004), this idea has never been evaluated in a morphologically dynamic river corridor for which a meter-scale digital elevation model is available across a wide range of discharges, from a fraction of to orders of magnitude more than bankfull. The goal of this study was to understand if and how bed elevation and flow-dependent channel width are organized in a partially confined, incising, regulated gravel–cobble bed river with multiple spatial scales of landform heterogeneity across a range of discharges. The analysis of geometric organization was accomplished through a suite of spatial series analyses using a 9 km reach of the lower Yuba River (LYR) in California, USA, as a test bed. Our central hypothesis is that the test river reach will have covarying and quasiperiodic bed and width oscillations. Due to the test river corridor’s variability (White et al., 2010), past history (James et al., 2009), and a Mediterranean climate (Wolman and Gerson, 1978), these patterns may be dominant in a range of flows. Knowledge of spatial patterns is commonly used to infer the geomorphic processes that yielded those patterns (Davis, 1909; Thornbury, 1954) and/or what future processes will be driven by the current spatial structure of landforms (Leopold and Maddock, 1953; Schumm, 1971; Brown and Pasternack, 2014). However, such inferences rarely include transparent, objective spatial analysis of topographic structure, so this study demonstrates a new methodology accessible to most practitioners to substantiate the ideas behind the process–morphology linkages they envision to be driven by variability in topography. The results of the study contribute to basic knowledge by showing multiple layers of coherent structure between width and bed undulations, which alerts geomorphologists to the need to prioritize future research on the cause and consequences of structured channel variability as opposed to further work on the central tendency of morphological metrics.

### 1.1 Background

A multitude of numerical, field, and theoretical studies have shown that gravel bed rivers have covarying oscillations between bed elevation and channel width related to riffle–pool maintenance processes. The joint periodicity in oscillating thalweg and bankfull width series for pool–riffle sequences in gravel bed rivers was identified by Richards (1976b), who noted that riffles have widths that are on average greater than those of pools, and he attributed this to flow deflection over riffles into the channel banks. Since then, many studies related to processes that rejuvenate or maintain the relief between bars and pools (i.e., “maintenance” or “self-maintenance”) have implied a specific spatial correlation of width and depth between the pool and riffle at the bankfull or channel-forming discharge (e.g., Wilkinson et al., 2004; MacWilliams et al., 2006; Caamano et al., 2009; Thompson, 2010). For example, Caamano et al. (2009) derived a criterion for the occurrence of a mean reversal in velocity

(Keller, 1971) that implies a specific correlation of the channel geometry of alluvial channels with undulating bed profiles. Specifically, for a reversal in mean velocity at the bankfull or channel-forming discharge (holding substrate composition constant), the riffle must be wider than the pool and the width variation should be greater than the depth variation between the riffle and residual pool depth. Milan et al. (2001) evaluated several riffle–pool couplets, from a base flow to just over the bankfull discharge. They found that convergence and reversals in section-averaged velocity and shear stress were complex and nonuniform, which suggests that different morphologic units may be maintained at different discharges. Wilkinson et al. (2004) explicitly showed that phase shifts in shear stress from the riffle to the pool between high and low discharge required positively covarying bed and width undulations. White et al. (2010) showed how valley width oscillations influence riffle persistence despite larger channel-altering floods and interdecadal valley incision. Sawyer et al. (2010) used two-dimensional (2-D) hydrodynamic modeling and digital elevation model (DEM) differencing to illustrate how variations in wetted width and bed elevation can modulate regions of peak velocity and channel change at a pool–riffle–run sequence across a range of discharges from 0.15 to 7.6 times bankfull discharge. DeAlmeida and Rodriguez (2012) used a 1-D morphodynamic model to explore the evolution of riffle–pool bedforms from an initially flat bed while maintaining the channel width variability. The resulting simulations were in close agreement to the actual bed profile in their model. Thus, their study is another example that channel width can exert controls on the structure of the bed profile. The flows at which the above processes are modulated vary in the literature.

From a system perspective, bed and width undulations, both jointly and in isolation, are a means of self-adjustment in alluvial channels that minimize the time rate of potential energy expenditure per unit mass of water in accordance with the law of least time rate of energy expenditure (Langbein and Leopold, 1962; Yang, 1971; Cherkauer, 1973; Wohl et al., 1999). For bed profiles, Yang (1971) and Cherkauer (1973) showed that undulating bed relief is a preferred configuration of alluvial channels that minimize the time rate of potential energy expenditure. Using field, flume, and numerical methods, Wohl et al. (1999) showed that valley wall oscillations also act to regulate flow energy analogous to bedforms. In analyzing reach-scale energy constraints on river behavior, Huang et al. (2004) quantitatively showed that wide and shallow sections and deep and narrow sections are two end member cross-sectional configurations necessary for efficiently expending excess energy for rivers, so these two types of cross sections imply covarying bed and width undulations as a means of expending excess energy. Therefore, the above studies suggest that both bed and width oscillations are a means to optimize channel geometry for the dissipation of excess flow energy. The question now is the extent to which this well-developed theory plays out in real

ivers, especially now that meter-scale river digital elevation models (DEMs) are available.

Flows that drive channel maintenance in western US rivers, such as the test river in this study (described in detail in Sect. 3 below), are thought to typically have recurrence intervals ranging from 1.2 to 5 years (Williams, 1978; Andrews, 1980; Nolan et al., 1987). Most of the literature investigating riffle–pool maintenance discussed above report bedform-sustaining flow reversals occurring at or near bank-full, often with no specificity to the frequency of these events (Lisle, 1979; Wilkinson et al., 2004). Studies that do report recurrence intervals have ranged from the 1.2- to 7.7-year recurrence flows (Keller, 1971; Sawyer et al., 2010). However, many rivers exhibit multiple scales of freely formed and forced landscape heterogeneity that should influence fluvial geomorphology when the flow interacts with them, no matter the magnitude (Church, 2006; Gangodagamage et al., 2007). For example, Strom and Pasternack (2016) showed that the geomorphic setting can influence the stage at which reversals in peak velocity occur. In their study an unconfined anastomizing reach experienced velocity reversals at flows ranging from 1.5- to 2.5-year recurrence flows, compared to 2.5- to 4.7-year recurrence flows for a valley-confined reach. Given that river geometry can record memory from past floods (Yu and Wolman, 1987) and the presence of multiple layers of topographic variability (Brown and Pasternack, 2014), it is hypothesized that covarying bed and width undulations could also be present at discharges other than bank-full.

## 1.2 Study objectives

The primary objectives of this study were to determine if there are covarying bed and width oscillations in the test reach, if they exhibit any periodicity, and how they vary with discharge. Based on the literature review above, we hypothesize there will be covarying bed and width oscillations that form quasiperiodic patterns, with the strongest relationship occurring for a broad range of channel-forming flows. A secondary objective is to demonstrate how a geomorphic covariance structure (GCS) analysis of minimum bed elevation and wetted width, as defined below, can be generated from high-resolution topography and hydraulic models to assess flow-dependent spatial organization of river corridor topography. The study site was a 6.4 km section of the lower Yuba River (LYR), an incising and partially confined self-formed gravel–cobble-bedded river (Fig. 1; described in Sect. 3). Several statistical tests were used on the serial correlation of minimum bed elevation,  $Z$ , channel top width,  $W^j$ , and their geomorphic covariance structure,  $C(ZW^j)$ , where  $j$  indexes the flow discharge. The novelty of this study is that it provides the first assessment of covarying bed and width oscillations in a partially confined, self-maintained alluvial river across a wide array of flows. The broader impact is that it provides a framework for analyzing the flow-dependent topographic

**Table 1.** Flows analyzed and their approximate recurrence intervals.

$Q$ ( $\text{m}^3 \text{s}^{-1}$ )	Approximate recurrence interval
8.50	1
28.32	1.03
141.6	1.2
283.2	1.5
597.5	2.5
1195	4.7
2390	12.7
3126	20

variability of river corridors, without differentiating between discrete landforms such as riffles and pools. Further, an understanding of the flow-dependent spatial structure of bed and width GCS would be useful in assessing their utility in applied river corridor analysis and synthesis for river engineering, management, and restoration.

## 2 Experimental design

To evaluate covarying bed and width undulations, the concepts and methods of geomorphic covariance structures were used (Brown, 2014; Brown and Pasternack, 2014). A GCS is a bivariate spatial relationship amongst or between variables along a pathway in a river corridor. It is not a single metric as in statistical covariance, but a spatial series, and hence can capture spatially explicit geomorphic structure. Variables assessed can be flow-independent measures of topography (e.g., bed elevation, centerline curvature, and cross section asymmetry) and sediment size as well as flow-dependent hydraulics (e.g., top width, depth, velocity, and shear stress; Brown, 2014), topographic change, and biotic variables (e.g., biomass and habitat utilization). Calculation of a GCS from paired spatial series is straightforward by the product  $x_{\text{std},i} \times y_{\text{std},i}$ , where the subscript “std” refers to standardized and possibly detrended values of two variables  $x$  and  $y$  at location  $i$  along the centerline, creating the serial data set  $C(XY)$ . Since this study is concerned with bed- and flow-dependent top width undulations, the GCS series at each flow  $j$  is denoted as  $C(ZW^j)$ . For simplification in this paper local values use similar notation and are differentiated by sentence context. More information on GCS theory is provided in Sect. 4.2 below. GCS series were generated for eight flows ranging from 8.50 to 3126  $\text{m}^3 \text{s}^{-1}$ , spanning a broad range of flow frequencies (Table 1). The range of selected flows spans a low-flow condition up to the flow of the last large flood in the river. These flows were selected to provide enough resolution to glean flow-dependent effects while not producing redundant results.

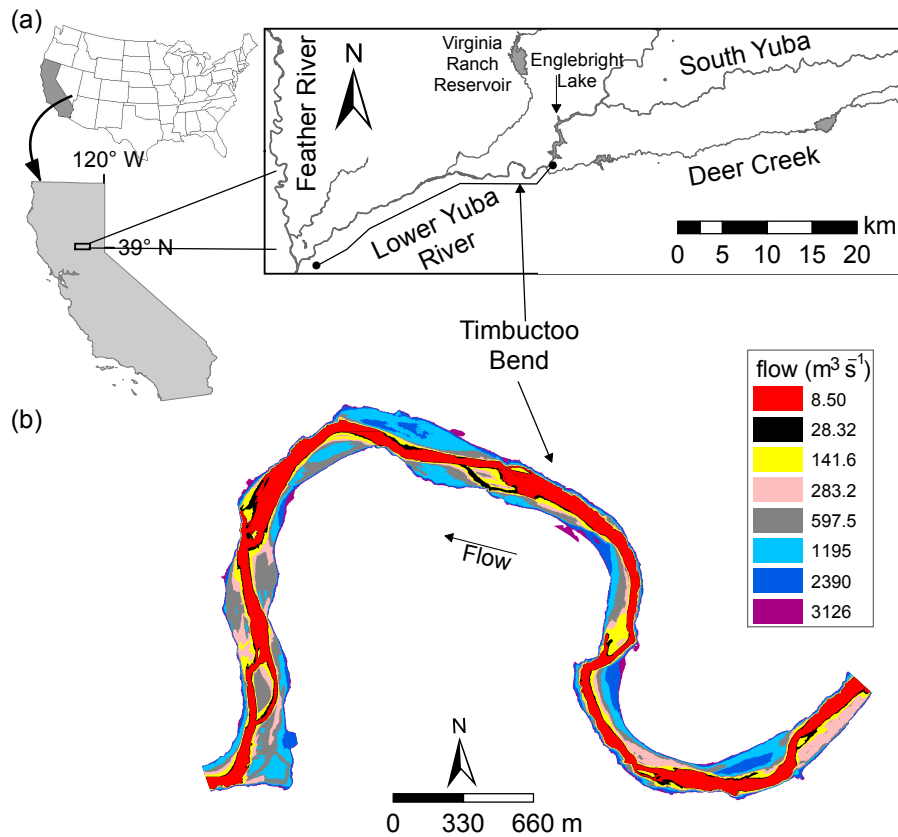


**Figure 1.** Regional and vicinity map of the lower Yuba River (a) and extent of study segment showing inundation extents predicted by the 2-D model (b).

The first question this study sought to answer was whether there was a tendency towards covarying  $Z$  and  $W^j$  and how it changed with discharge. If  $Z$  and  $W^j$  covary, then the sign of the residuals of both variables will be positive or negative, yielding a positive  $C(ZW^j) > 0$ . Therefore, to determine if there are covarying bed and width oscillations, a histogram was generated for each flow-dependent series of  $C(ZW^j)$ . The second question was whether each flow-dependent series of  $C(ZW^j)$  was random, constant, periodic, or quasiperiodic. Quasiperiodicity in this setting is defined as a series with periodic and random components, as opposed to purely random or purely periodic (Richards, 1976a). Quasiperiodicity differs from periodic series in that there are elements of randomness blended in (Newland, 1993). To answer this question autocorrelation function (ACF) and power spectral density (PSD) analyses of each  $C(ZW^j)$  series were used to determine if there were statistically significant quasiperiodic length scales (sensu Carling and Orr, 2002) at which  $C(ZW^j)$  covary and how that changes with discharge.

Based on the studies listed above (Sect. 1.1), we hypothesize that gravel–cobble-bedded rivers capable of rejuvenating their riffle–pool relief should exhibit a topography (at any instant in time) with a tendency towards quasiperiodic and covarying bed and width oscillations. The basis for covary-

ing and quasiperiodic bed and width oscillations is founded on the idea that, on average, channel geometry is maintained during bankfull (e.g., geometric bankfull) discharge and that locally channels are shaped by riffle–pool maintenance mechanisms (Wilkinson et al., 2004; MacWilliams et al., 2006; Caamano et al., 2009; Thompson, 2010). Based on the literature reviewed in Sect. 1.1, we hypothesize that the  $C(ZW^j)$  GCS will, on average, become more positive with increasing flow until approximately the bankfull discharge, where the channel overtops its banks and non-alluvial floodplain features exert control on cross-sectional mean hydraulics. At that point there may not be a tendency towards positive or negative residuals if the topographic controls at that flood stage are not important enough to control channel morphology. For example, smaller events might occur frequently enough to erase the in-channel effects of the large infrequent events, especially in a temperate climate (Wolman and Gerson, 1978). On the other hand, if a system is dominated by the legacy of a massive historical flood and lacks the capability to recover under more frequent floods, then the  $C(ZW^j)$  GCS will continue to increase positively until the discharge that carved out the existent covarying bed and width oscillations for the current topography is revealed. Note that we do not expect a clear threshold where organiza-

tion in the  $C(ZW^j)$  GCS is a maximum but rather a range of flows near the bankfull discharge. The effect of a particular flow on a channel is dependent not just on that flow but on the history of flow conditions that led to the channel's condition (Yu and Wolman, 1987). Therefore, it should not be expected that the observed patterns will be associated with a singular flow value. Also, this study looked at a river in a Mediterranean climate, and thus it may be more prone to exhibiting a wider range of positive  $C(ZW^j)$  GCS than a temperate or tropical river, as the number and frequency of recovery processes is reduced (Wolman and Gerson, 1978). With this logic, it is hypothesized that the  $C(ZW^j)$  GCS will be quasiperiodic for flows near the bankfull discharge, due to the presence of bar and pool topography, and that the ACF and PSD will yield length scales commensurate with the average spacing of these topographic features. For flows above the bankfull discharge, a river corridor has many local alluvial landforms, bedrock outcrops, and artificial structures on its floodplain and terraces. These features influence bed adjustment during floods that engage them and hence impact the GCS. It is unknown how GCS length scales will change in response to the topographic steering these features induce, causing changes to bed elevation, but investigating that is a novel and important aspect of this study. In addition to performing these tests, we also present two  $\sim 1.4$  km sections of the  $C(ZW^j)$  GCS,  $Z$ ,  $W$ , and the detrended topography for three representative flows to discuss specific examples of how these patterns change with landforms in the river corridor across a wide array of discharges.

Limitations to this study (but not the GCS approach) for worldwide generalization include not considering other variables relevant to how alluvial rivers adjust their shape, such as grain size, channel curvature, and vegetation, to name a few. Some of these limitations were not study oversights but reflected the reality that the study reach used had relatively homogenous sediments (Jackson et al., 2013), low sinuosity, and limited vegetation (Abu-Aly et al., 2014). This yielded an ideal setting to determine how much order was present for just bed elevation and channel width but does not disregard the importance of these other controls, which can be addressed in future studies at suitable sites. Also, this study is not a direct test of the response to or drivers of morphodynamic change. The extent to which GCS can be used as an indicator of change to simplify geomorphic analysis instead of doing morphodynamic modeling remains unknown, but finding metrics that link landforms, the agent that shape them, and the responses they induce has always been the goal of geomorphology (Davis, 1909).

### 3 Study area

#### 3.1 River context

The study area was the 6.4 km Timbuctoo Bend reach of the lower Yuba River (LYR) in northeastern California, USA.

The reach begins at the outlet of a bedrock canyon that is dammed  $\sim 3$  km upstream, and the watershed above the dam drains 3480 km<sup>2</sup> of dry summer subtropical mountains. Little is known about the pre-European Yuba River, but in this reach it is confined by valley hillsides and bedrock outcrops, and these are evident in some photos from early European settlers panning the river for gold in the late 1840s. During the mid to late 19th century there was a period of extensive hydraulic gold mining of hillside alluvial deposits in the upper Yuba watershed that delivered an overwhelming load of heterogeneous sediment to the lowland river valley (James et al., 2009). Geomorphologist G. K. Gilbert photo-documented the LYR around the time of its worst condition in the early 20th century and provided foundational thinking related to how the river would evolve in time (Gilbert, 1917). In 1941 Englebright Dam was built to hold back further sediment export from the mountains, and that allowed the river valley to begin a process of natural recovery, which was reviewed by Adler (1980) and more recently by Ghoshal et al. (2010). However, this process was interfered with by widespread dredger mining in the early to mid 20th century. In two locations of the study reach there are wide relict dredger tailings piles on the inside of the two uppermost meander bends that the river has been gradually eroding.

The hydrology of the regulated LYR is complex and quite different from the usual story of significantly curtailed flows below a large dam. Englebright Dam primarily serves as a sediment barrier, and it is kept nearly full. As a result, it is operated to overtop when outflow is  $> 127.4$  m<sup>3</sup> s<sup>-1</sup>, long enough to fill its small remaining capacity, so flood hydrology is still seasonal and driven by rainfall and snowmelt in the watershed. Two of three sub-catchments do not have large dams, so winter floods and spring snowmelt commonly cause spill over Englebright sufficient to exceed the bankfull channel in Timbuctoo Bend. The one regulated sub-catchment does have a large dam, New Bullards Bar (closed in 1970), and this reduces the frequency and duration of floodplain inundation compared to the pre-dam record (Escobar-Arias and Pasternack, 2011; Cienicala and Pasternack, 2016), but it is not like other rivers where the entire upstream watershed is regulated. Sawyer et al. (2010) reported the 1.5-year recurrence interval for the post-Englebright, pre-New Bullards Bar period as 328.5 m<sup>3</sup> s<sup>-1</sup> and then for post-New Bullards Bar as 159.2 m<sup>3</sup> s<sup>-1</sup>. California has long been known to exhibit a roughly decadal return period for societally important major floods that change river courses (Guinn, 1890), though the magnitude of those floods is not necessarily a 10-year recurrence interval scientifically. Since major flow regulation in 1970, the three largest peak annual daily floods came roughly 10 years apart, in the 1986, 1997, and 2006 water years. The flood of 1997 was the largest of the post-dam record. The 2006 peak flood event had a recorded peak 15 min discharge of 3126.2 m<sup>3</sup> s<sup>-1</sup> entering the study reach.

Wyrick and Pasternack (2012) analyzed LYR inundation patterns in a high-resolution DEM of the river produced af-

ter the 2006 wet season, and they considered how channel and floodplain shapes change dramatically through the study reach. Their findings apply to the Timbuctoo Bend reach. Different locations exhibited spillage out of the channel into low-lying peripheral swales and onto lateral and point bars at flows from  $\sim 84.95\text{--}141.6\text{ m}^3\text{ s}^{-1}$ . When the water stage rises to  $141.6\text{ m}^3\text{ s}^{-1}$ , relatively flat active bar tops become inundated and the wetted extents line up with the base of willows along steeper banks flanking the channel. These and other field indicators led to the consideration of  $141.6\text{ m}^3\text{ s}^{-1}$  as representative of the bankfull discharge adjusted to the modern regulated flow regime since 1970. By a flow of  $198.2\text{ m}^3\text{ s}^{-1}$ , banks are all submerged and water is spilling out to various degrees onto the floodplain. The floodplain is considered fully inundated when the discharge reaches  $597.5\text{ m}^3\text{ s}^{-1}$ . Above that flow stage exist some terraces, bedrock outcrops, and soil-mantled hillsides that become inundated. Regarding the two relict dredger tailings piles mentioned earlier, they interact with the flows ranging from  $597.5\text{--}1,195\text{ m}^3\text{ s}^{-1}$ . Apart from these piles, the flow width interacts predominately with the valley walls for discharges at  $1195\text{ m}^3\text{ s}^{-1}$  and above. Given the estimate of bankfull discharge for the LYR, the instantaneous peak flow during the 2006 flood was  $\sim 23$  times that, so quite substantial compared to those commonly investigated in modern geomorphic studies.

### 3.2 Timbuctoo Bend details

A lot is known about the geomorphology of Timbuctoo Bend, and this information helps inform this study to substantiate the possibility that the river's topography is organized in response to differential topographic steering as a function of flow stage. According to Wyrick and Pasternack (2012), the reach has a mean bed slope of 0.002, a thalweg length of 6337 m, a mean bankfull width of 84 m, a mean floodway width of 134 m, an entrenchment ratio of 2.1 (defined per Rosgen, 1996), and a weighted mean substrate size of 164 mm. Using the system of Rosgen (1996), it classifies as a B3c stream, indicating moderate entrenchment and bed slope with cobble channel material. A study of morphological units revealed that its base flow channel area consists of 20 % pool, 18 % riffle, and then a mix of six other landform types. More than half of the area of the riverbank ecotone inundated between base flow and bankfull flow is composed of lateral bars, with the remaining area containing roughly similar areas of point bars, medial bars, and swales (Wyrick and Pasternack, 2012). A study of bankfull channel substrates found that they are differentiated by morphological unit type, but the median size of all units is in the cobble range (Jackson et al., 2013), even depositional bars that are often thought of as relatively fine in other contexts. Vegetated cover of the river corridor ranged from 0.8 to 8.1 % of the total wetted area at each flow, with more inundated vegetation at higher flows.

White et al. (2010) used a sequence of historical aerial photos, wetted channel polygons, repeat long profiles from 1999 and 2006, and a valley width series to conclude that even though Timbuctoo Bend has incised significantly since 1942 in response to many floods, there are several riffles and pools that persist in the same wide and constricted valley locations, suggesting that valley width oscillations maintain those positions and drive morphodynamic response. This suggests that it may not matter exactly which instant topography one might analyze to look at the effect of topographic variability in controlling or responding to large flood processes, as they all should reflect the same topographic steering regime induced by the valley walls.

Two studies have been done to look at the hydraulic processes associated with different flood stages in Timbuctoo Bend. Sawyer et al. (2010) found that one of the pool–riffle–run units in this reach experienced flow convergence routing between baseflow, bankfull flow, and a flow of roughly 8 times bankfull discharge that maintained riffle relief. Strom et al. (2016) assessed the hydraulics of the whole reach over the same range of flows in this study, and they reported that the reach exhibits a diversity of stage-dependent shifts in the locations and sizes of patches of peak velocity. The spatial persistence of such patches decreased with discharge until flows exceeded  $\sim 1000\text{ m}^3\text{ s}^{-1}$ , at which point valley walls sustained their location for flows up to the peak of  $3126\text{ m}^3\text{ s}^{-1}$ . Also, peak velocity patches resided preferentially over chute and riffle landforms at within-bank flows, several morphological unit types landforms for small floods, and pools for floods  $> 1000\text{ m}^3\text{ s}^{-1}$ . These studies corroborate the process inferences made by White et al. (2010) in that hydraulics were found to be stage-dependent in ways that were consistent with the mechanism of flow convergence routing.

Finally, Carley et al. (2012), Wyrick and Pasternack (2015), and Pasternack and Wyrick (2016) used DEM differencing, uncertainty analysis, scale-stratified sediment budgeting, and topographic change classification to analyze how the LYR changed from 1999 to 2008, including Timbuctoo Bend. These studies took advantage of the repeated mapping of the LYR in 1999 and 2006–2008, with Timbuctoo Bend mapped entirely in 2006. They found large amounts of erosion and deposition, strong differential rates of change among different landforms on three spatial scales, and topographic changes driven by 19 different geomorphic processes. For Timbuctoo Bend, the dominant topographic change processes found were in-channel downcutting (including knickpoint migration) and overbank (i.e., floodplain) scour, with noncohesive bank migration a distant third. Thus, the river appears to change through adjustments to its bed elevation far more than changes to its width in this reach. This finding will come into play in interpreting the results of this study later on.

In summary, even with modern technology it is impossible to monitor the hydrogeomorphic mechanics of fluvial change

in a large river for flows up to 22 times bankfull discharge, so recent studies have tried to get at the mechanisms during such events with a range of strategies. Historical river analysis, hydrodynamic modeling, and topographic change detection and analysis have been used together to reveal a picture of a river that is changing in response to multiple scales of landform heterogeneity that drive topographic steering. Even though the river has changed through time, there has been a persistence of nested landforms, and thus it would be useful to understand how topographic features are organized purely through an analysis of the DEM per the methods developed in this study. This study exclusively uses the 2006 map made during the dry season that followed the dramatic 2006 wet season, which included the large flood, two other notable peaks, and a total of 18 days of floodplain filling flow. Thus, it addresses the topography as it existed after that river-altering wet season and how it will in turn influence the dynamics of the next one.

## 4 Methods

The meter-scale topographic map of Timbuctoo Bend produced from echosounder and robotic total station ground surveys was used for extraction of  $Z$  (Carley et al., 2012; see Supplement), while a corresponding meter-scale 2-D hydrodynamic model was used to generate data sets for  $W^j$  for each discharge. Details about the 2-D model are documented in the Supplement and previous publications (Abu-Aly et al., 2013; Wyrick and Pasternack, 2014; Pasternack et al., 2014); it was thoroughly validated for velocity vector and water surface elevation metrics, yielding outcomes on par with or better than other publications using 2-D models.

### 4.1 Data extraction

A first step was to extract  $Z$  and  $W^j$  spatial series from the digital elevation model and 2-D model outputs. This required having a sample pathway along which bed elevation could be extracted from the DEM and top width from the wetted extents from the 2-D model. Sampling river widths was done using cross sections generated at even intervals perpendicular to the sample pathway and then clipped to the 2-D model-derived wetted extent for each flow. Because of this, the pathway selected can have a significant bearing on whether or not sample sections represent downstream-oriented flow or overlap where pathway curvature is high. There are several options in developing an appropriate pathway for sampling the river corridor. The thalweg is commonly used in flow-independent geomorphic studies, but the thalweg is too tortuous within the channel to adhere to a reasonable definition of top width. Further, as flow increases, central flow pathway deviates from the deepest part of the channel due to higher flow momentum and topographic steering from submerged and partially submerged topography (Abu-Aly et al., 2014). Therefore, in this study we manually developed flow-

dependent sample pathways using 2-D model hydraulic outputs of depth, velocity, and wetted area. The effect of having different sample pathways for each flow is that it accounts for flow steering by topographic features in the river corridor.

For each flow a grid of kinetic flow energy ( $d_i \times v_i^2$ ) was generated in ARCGIS<sup>®</sup>, where  $d_i$  is the depth and  $v_i$  is the velocity at node  $i$  in the 2-D model hydraulics rasters. Then a sample pathway was manually digitized using the momentum grid, following the path of greatest kinetic energy. For flow splits around islands, if the magnitude of energy in one channel was more than twice as great as the other, it was chosen as the main pathway. If they were approximately equal, then the pathway was centered between the split. Once a sample pathway was developed, it was then smoothed using a Bezier curve approach over a range of 100 m or approximately a bankfull channel width to help further minimize section overlaps. For each sample pathway, cross sections were generated at 5 m intervals and clipped to the wetted extent of each flow, with any partially disconnected backwater or non-downstream-oriented areas manually removed.

Despite smoothing there were areas of the river where the river has relatively high curvature in the sample pathway, causing sample section overlaps to occur. These were manually edited by visually comparing the sample sections with the kinetic flow energy grid and removing overlapped sections that did not follow the downstream flow of water. This was more prevalent at the lower discharges than the higher ones due to the effects topographic steering creating more variable sample pathways.

To provide a constant frame of spatial reference for comparison of results between flows, while preserving flow-dependent widths, sections were mapped to the lowest flow's sample pathway using the spatial join function in ARCGIS<sup>®</sup>. The lowest flow was used because that had the longest path. This ensures no multiple-to-one averaging of data would happen, as that would otherwise occur if data were mapped from longer paths to shorter ones. To create evenly spaced spatial series the data were linearly interpolated to match the original sampling frequency of 5 m. Minimum bed elevation along each section was sampled from the DEM using the same sections for measuring width for the lowest-flow sample pathway.

### 4.2 Developing geomorphic covariance structures

To generate GCS series for bed- and flow-dependent width undulations, the two variables,  $Z$  and  $W^j$ , were first detrended and standardized. Detrending is not always needed for width in GCS analysis, but some analyses in this study did require it. A linear model was used for  $Z$ , (Table 2) as is common in many studies that analyze reach-scale bed variations (Melton, 1962; Richards, 1976a; McKean et al., 2008). Similarly, each  $W^j$  series was linearly detrended, but the trends were extremely small, with a consistent slope of just 0.002 (Table 2). Finally, each series was standardized by

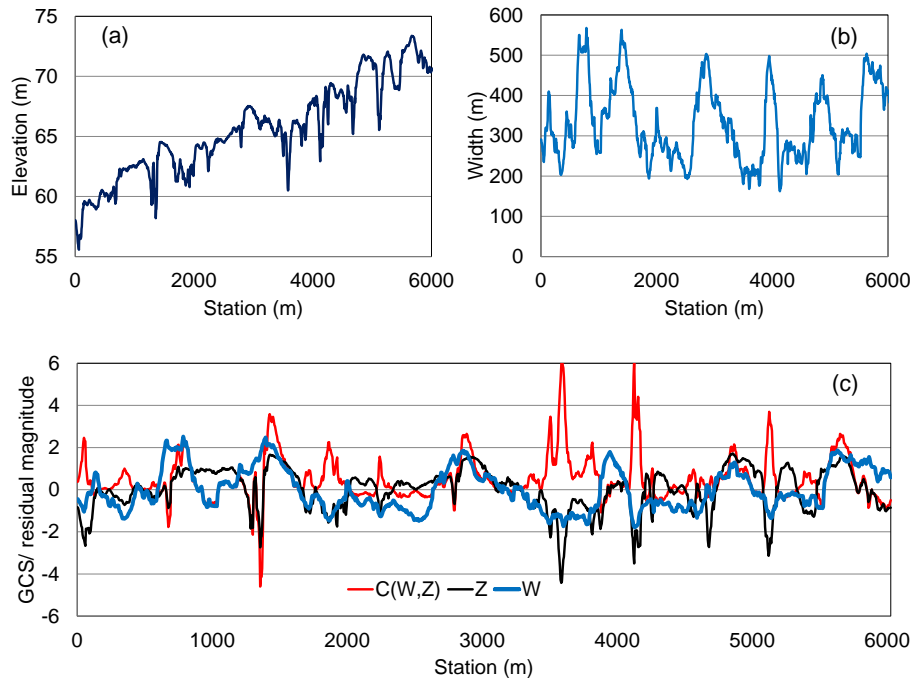


**Figure 2.** Raw bed profile (a) and flow width (b) series for  $283.2 \text{ m}^3 \text{ s}^{-1}$ . After detrending and standardizing, values of  $Z$  (black line in c) and  $W$  (blue line in c) are multiplied together to compute  $C(ZW^j)$  (red line in c). The whole series of  $C(ZW^j)$  is the GCS.

the mean and variance of the entire detrended series (Salas et al., 1980) to achieve second-order stationarity, which is a prerequisite for spectral analysis (described in the following section). Second-order stationarity of a series means that the mean and variance across the domain of analysis are constant (Newland, 1983). Removal of the lowest frequency of a signal, which can often be visually assessed, has little impact upon subsequent spectral analyses (Richards, 1979). A linear trend was used over other options such as a polynomial because a linear trend preserves the most amount of information in the bed series, while a polynomial can filter out potential oscillations. After detrended and standardized series of  $Z$  and  $W^j$  were generated, then the GCS between them was computed by taking the product of the two at each centerline station, yielding a spatially explicit measure of how the two covary (Fig. 2). The GCS is the whole series of  $C(ZW^j)$  values and not a single metric such as the traditional statistical definition of covariance. Interpretation of a GCS is based on the sign, which in turn is driven by the signs of contributing terms. For  $C(ZW^j)$ , if both  $Z$  and  $W^j$  are positive or negative, then  $C(ZW^j) > 0$ , but if only one is negative then  $C(ZW^j) < 0$ . These considerations yield four sub-reach-scale landform end members that deviate from normative conditions (Fig. 3). Normal conditions in this context refer to areas where both variables are close to the mean and thus  $C(ZW^j) \sim 0$ . Note that the signs of  $Z$  and  $W^j$  are not only important, but the magnitude is, too. Since  $C(ZW^j)$  is generated by multiplication, if either  $Z$  or  $W^j$  is within the

range of  $-1$  to  $1$ , then it serves to discount the other. If  $Z$  or  $W^j$  is  $> 1$  or  $< -1$ , it amplifies  $C(ZW^j)$ . We did not assess the statistical significance of coherent landform patterns, but one could do so following Brown and Pasternack (2014).

### 4.3 Data analysis

Before any statistical tests were performed, we first visually assessed the data in two approximately 1.4 km long sections to illustrate how  $C(ZW^j)$  is affected by flow responses to landforms. For these two examples only three discharges were selected to illustrate flow-dependent changes in  $Z$ ,  $W^j$ , and  $C(ZW^j)$  with fluvial landforms. The lowest and highest flows, i.e.,  $8.50$  and  $3126 \text{ m}^3 \text{ s}^{-1}$ , were selected to bracket the range of flows investigated. The intermediate flow selected was  $283.2 \text{ m}^3 \text{ s}^{-1}$  based on the shifts in  $C(ZW^j)$  observed in the histogram, ACF, and PSD tests as shown below in the results. For these examples the exact magnitudes of  $C(ZW^j)$  are not as important as the patterns and how they relate to visually discernible landforms.

A Mann–Whitney  $U$  test was performed between each  $C(ZW^j)$  data set to determine if they were statistically different at the 95 % level. Histograms were then computed for each  $C(ZW^j)$  data set to evaluate whether there was a tendency for the data to be positively covarying and how that changes with discharge. Two histograms were developed, one based on the quadrant classification of  $C(ZW^j)$  for each flow and another showing the  $C(ZW^j)$  magnitude. This was done so that the distribution of both the type of  $C(ZW^j)$

**Table 2.** Linear trend models and  $R^2$  for  $Z$  and  $W^j$  used in detrending each series.

Discharge ( $\text{m}^3 \text{s}^{-1}$ )	Top width	$R^2$	Bed elevation	$R^2$
	Linear trend model		Linear trend model	
8.50	$y = -0.0016x + 193.03$	0.0231	$y = 0.002x + 194.2$	0.8727
28.32	$y = -0.0025x + 234.27$	0.0429	$y = 0.002x + 194.26$	0.8713
141.6	$y = -0.003x + 301.61$	0.0423	$y = 0.0021x + 194.04$	0.8731
283.2	$y = -0.0002x + 332.87$	0.0002	$y = 0.0021x + 194.23$	0.8710
597.5	$y = -0.0101x + 528.6$	0.2286	$y = 0.0021x + 194.16$	0.8711
1195	$y = -0.0133x + 665.02$	0.3037	$y = 0.0021x + 194.29$	0.8703
2390	$y = -0.012x + 710.57$	0.2420	$y = 0.0022x + 193.92$	0.8736
3126	$y = -0.0121x + 733.12$	0.2437	$y = 0.0022x + 193.94$	0.8733

and magnitudes could be assessed. Additionally, the bivariate Pearson's correlation coefficients ( $r$ ) were computed between  $Z$  and  $W^j$  to assess their potential interdependence. Bivariate Pearson's correlation coefficients were also computed each series of  $W^j$ . Statistical significance was assessed for ( $r$ ) using a white-noise null hypothesis at the 95 % level.

Next, ACF and PSD analyses were used to determine if  $C(ZW^j)$  was quasiperiodic or random, as it was visually evident that it was not constant or strictly periodic. If a series is quasiperiodic, this will be reflected in statistically significant periodicity in the ACF (Newland, 1993; Carling and Orr, 2000). Because the PSD is derived from the ACF the two tests show the same information but in different domains, with the ACF in the space domain and the PSD in the frequency domain. So while the ACF analysis reveals periodicity in the signal (if present), the PSD analysis presents the associated frequencies. Both are shown to visually reinforce the results of the PSD analysis. This is helpful because spectral analysis can be very sensitive to the algorithm used and associated parameters such as window type and size. Showing the ACF allows a visual check of dominant length scales that may have quasiperiodicity (e.g., as in Carling and Orr, 2000). The ACF analysis was performed for each flow-dependent series of  $C(ZW^j)$ , and then these were compared among flows to characterize stage-dependent variability and to analyze how spatial structure changed with discharge. This test essentially determines the distances over which  $C(ZW^j)$  are similar. An unbiased estimate of autocorrelation for lags was used:

$$R_k = \frac{n}{n-k} \frac{\sum_{i=1}^{n-k} (x_i - \bar{x})(x_{i+k} - \bar{x})}{\sum_{i=1}^{n-k} (x_i - \bar{x})^2}, \quad (1)$$

where  $x_i$  is a value of a GCS series at location  $i$ ,  $\bar{x}$  is the mean value of the GCS (zero due to standardization process), and the terms  $\frac{1}{n-k}$  and  $\frac{1}{n}$  account for sample bias (Cox, 1983; Shumway and Stoffer, 2006). Each  $R_k$  vs. lag series was plotted against discharge for a maximum of 640 lags (3.2 km, or approximately half the study length), creating a surface that

shows how ACF evolves with flow. Lag intervals are equal to sample interval for the data sets (e.g., 5 m). Statistical significance was assessed relative to both white- and red-noise autocorrelations. White noise is associated with random processes that are uncorrelated in space, while red noise is associated with data that have properties of first-order autocorrelation (Newland, 1993). The benefit of this approach is that (i) many fluvial geomorphic spatial series display autoregressive properties (Melton, 1962; Rendell and Alexander, 1979; Knighton, 1983; Madej, 2001) and (ii) it provides further context for interpreting results beyond assuming white-noise properties. The 95 % confidence limits for white noise are given by  $-\frac{1}{n} \pm \frac{2}{\sqrt{n}}$  (Salas et al., 1980). For red noise, a first-order autoregressive (AR1) model was fit to the standardized residuals for each spatial series of bed elevation and channel width. For comparison, first-order autoregressive (AR1) models were produced for 100 random spatial series (each with the same number of points as the flow width spatial series) and averaged. Each averaged AR1 flow width series was then multiplied with the AR1 bed elevation series to create an AR1 model for each  $C(ZW^j)$ . The red-noise estimate was then taken as the average of all AR1 models of  $C(ZW^j)$ . The ACF plots were made so that values not exceeding the white-noise significance are not shown, along with a reference contour for the AR1 estimate. Frequencies can be gleaned from the ACF analysis by taking the inverse of the lag-distance-associated repeating peaks following Carling and Orr (2002).

Power spectral density was estimated for each  $C(ZW^j)$  series using a modified periodogram method (Carter et al., 1973). The periodogram is the Fourier transform of the biased estimate of the autocorrelation sequence. The periodogram is defined as

$$P(f) = \frac{\Delta x}{N} \left| \sum_{n=0}^{N-1} h_n x_n e^{-i2\pi f n} \right|^2, \quad (2)$$

where  $P(f)$  is the power spectral density of  $x$ ,  $h_n$  is the window,  $\Delta x$  is the sample rate, and  $N$  is the number of data points (Trauth et al., 2006). While the raw periodogram can exhibit spectral leakage, a window can reduce this effect. A hamming window was used with a length equal to each

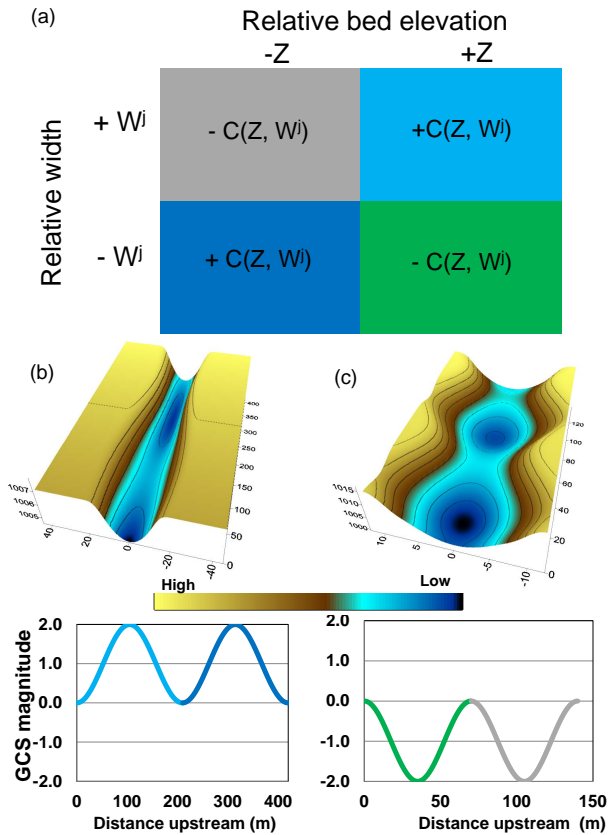


**Figure 3.** Conceptual key for interpreting  $C(ZW^j)$  geomorphic covariance structures (a). For quadrant 1,  $Z$  and  $W^j$  are both relatively high, so that implies wide and shallow areas associated with deposition. Conversely, in quadrant 2,  $Z$  is relatively low, but  $W^j$  is relatively high, which implies deep and wide cross areas, which in turn implies that these areas may have been scoured at larger flows. In quadrant 3,  $Z$  and  $W^j$  are both relatively low, so that implies narrow and deep areas associated with erosion. Finally, in quadrant 4,  $Z$  is relatively high and  $W^j$  is relatively low, so that implies narrow and topographically high areas. Prototypical channels and GCS with positive (b) and negative (c)  $C(ZW^j)$  colored according to (a).

data set. Since samples were taken every 5 m, this resulted in a sampling frequency of  $0.2 \text{ cycles m}^{-1}$  and a Nyquist frequency, or cutoff, of  $0.1 \text{ cycles m}^{-1}$ . The number of data points used for the analysis was roughly half the largest data set, resulting in a bandwidth of  $0.00016 \text{ cycles m}^{-1}$ . For PSD estimates a modified Lomb–Scargle confidence limit for white noise at the 95 % level was used as recommended by Hernandez (1996). Since this study was concerned with changes in PSD with flow, estimates were plotted relative to the standard deviation of all PSD results for all series. This was done instead of using the standard deviation of each series because that inflates power within a series without context for the variance of adjacent flows.

## 5 Results

### 5.1 Relating $C(ZW^j)$ patterns to landforms

The first example is located at the lower end of the study area and transitions from a valley meander to a straighter valley section with several valley corridor oscillations (Fig. 4). Starting upstream there is a large point bar on river left with a pool (i.e.,  $-Z$ ) that transitions to a broad riffle with a 200 m long zone with  $Z > 1$ . Downstream, the river channel impinges on the valley walls, creating two forced pools with localized negative spikes in  $Z$  (Fig. 4a, b). Downstream of this, the low-flow channel is steered to the left of the valley, being bounded by two bars. In this zone  $Z$  values are positive and  $\sim 1$ . Past this there is an inset anabranch that transitions to a constricted pool with a broad terrace on river left. In this lower zone,  $Z$  fluctuates between 0 and  $-1$ .

Given that bed elevation is held fixed for this type of analysis, changes in  $W^j$  act to modulate the sign and magnitude of the  $C(ZW^j)$  GCS with increasing flow. In particular, when  $Z$  is near a value of 1, the relative flow  $W$  modulates the sign and strength of the GCS signal, with several possible changes including persistence, shifting, reversal, and emergence. For example, a persistent positive  $W$  oscillation occurs near station 1500, where this zone is always relatively wide regardless of flow. The anabranch zone, however, shows the positive peak in  $W^j$  shift downstream from station 900 to 600 from  $8.5$  to  $283.2 \text{ m}^3 \text{ s}^{-1}$ . Two reversals in  $W^j$  occur from low to high flow near stations 350 and 1100, which also create reversals in the GCS, but with different signs. Near station 400,  $Z$  and  $W^j$  are negative at  $8.5$  and  $283.2 \text{ m}^3 \text{ s}^{-1}$ , creating a positive GCS. However,  $W^j$  increases with flow discharge with an emergent positive peak in  $W$  at  $3126 \text{ m}^3 \text{ s}^{-1}$ , which yields a negative GCS.

The other example area occurs at a transition from a valley bend to a straighter section where the river transitions from a broad point bar on river left and eventually crosses over between two smaller inset point bars (Fig. 5a, b). Starting at the upstream extent a large point bar is located on river left with two forced pools in the channel at approximately 3500 and 3600 that have the strongest negative spikes in  $Z$  (Fig. 5c, d). Downstream where the point bar ends, the bed profile increases over a broad riffle with  $Z > 1$  located above station 3000. As mentioned above in Sect. 3, this pool–riffle–run sequence was studied in great detail by Sawyer et al. (2010), who confirmed the occurrence of naturally rejuvenating riffle–pool topography. Immediately below the broad riffle is a localized zone where  $Z > 1$  adjacent to a small bedrock outcrop. Within the alternate bars the bed profile is between 0 and 1 for  $\sim 300$  m, followed by a localized negative peak in  $Z$  around station 2300.

For the first 200 m,  $W^j$  is  $< 0$  for all three flows but gradually increases downstream with increasing flow (Fig. 5c). Since the two deep pools in this initial zone have  $Z > 1$ , the GCS is  $> 1$  for all flows but reaches a maximum magni-

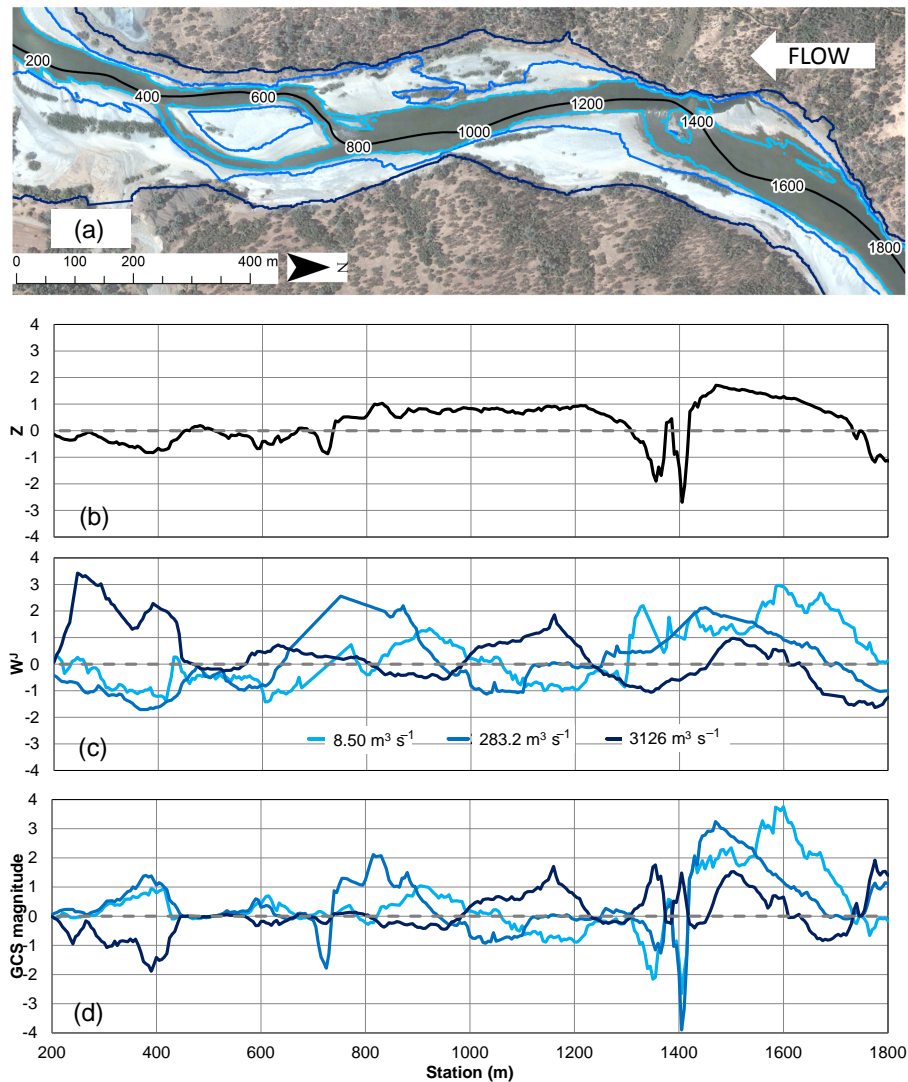


**Figure 4.** Example section in the middle of the study area showing inundation extents (a). Below are plots of minimum bed elevation (b), flow widths for  $8.50$ ,  $283.2$ , and  $3126 \text{ m}^3 \text{ s}^{-1}$  (c), and  $C(ZW^j)$  for the same flows. The aerial image is for a flow of  $21.29 \text{ m}^3 \text{ s}^{-1}$  on 28 September 2006.

tude of 6 at  $283.2 \text{ m}^3 \text{ s}^{-1}$ . Beyond this area  $W^j$  increases for all flows, but the relative peak broadens and shifts downstream with increasing discharge. At  $8.5 \text{ m}^3 \text{ s}^{-1}$  the peak is centered near station  $\sim 3000$ , where it appears that a back-water increases flow widths upstream of station 2900. For  $283.2 \text{ m}^3 \text{ s}^{-1}$  the peak shifts downstream  $\sim 150 \text{ m}$  as the anabranch becomes activated and begins to spread water out. At  $3126 \text{ m}^3 \text{ s}^{-1}$  the peak is shifted another  $\sim 300 \text{ m}$  downstream as the bounding point bars are inundated. These shifts in relative  $W^j$  act with the bed profile to create a sharper positive peak in  $C(ZW^j)$  near the riffle at low flows, but then this peak dampens and shifts downstream with increasing flow. There is a similar phase shifting reported for a mixed alluvial–bedrock riffle–pool unit reported by Brown and

Pasternack (2014), associated with a corresponding phasing of peak velocity from the riffle to the pool with increased flow. Given that the lower  $\sim 500 \text{ m}$  of this example area have  $Z \sim 0$ , the  $C(ZW^j)$ , GCS is also  $\sim 0$ .

Overall, both examples show that zones where  $Z$  was either  $> 1$  or  $< -1$  were associated with large pools and riffles in the study area and were characterized by strong peaks (e.g.,  $> 1$ ) in  $C(ZW^j)$ . Patterns of  $W^j$  can work with  $Z$  to create a variety of flow-dependent responses including emergence, reversals, amplification, and shifting. An interesting result is that most of the locations where  $Z < 1$  were short in length, whereas areas where  $Z > 1$  tended to be broader in length.

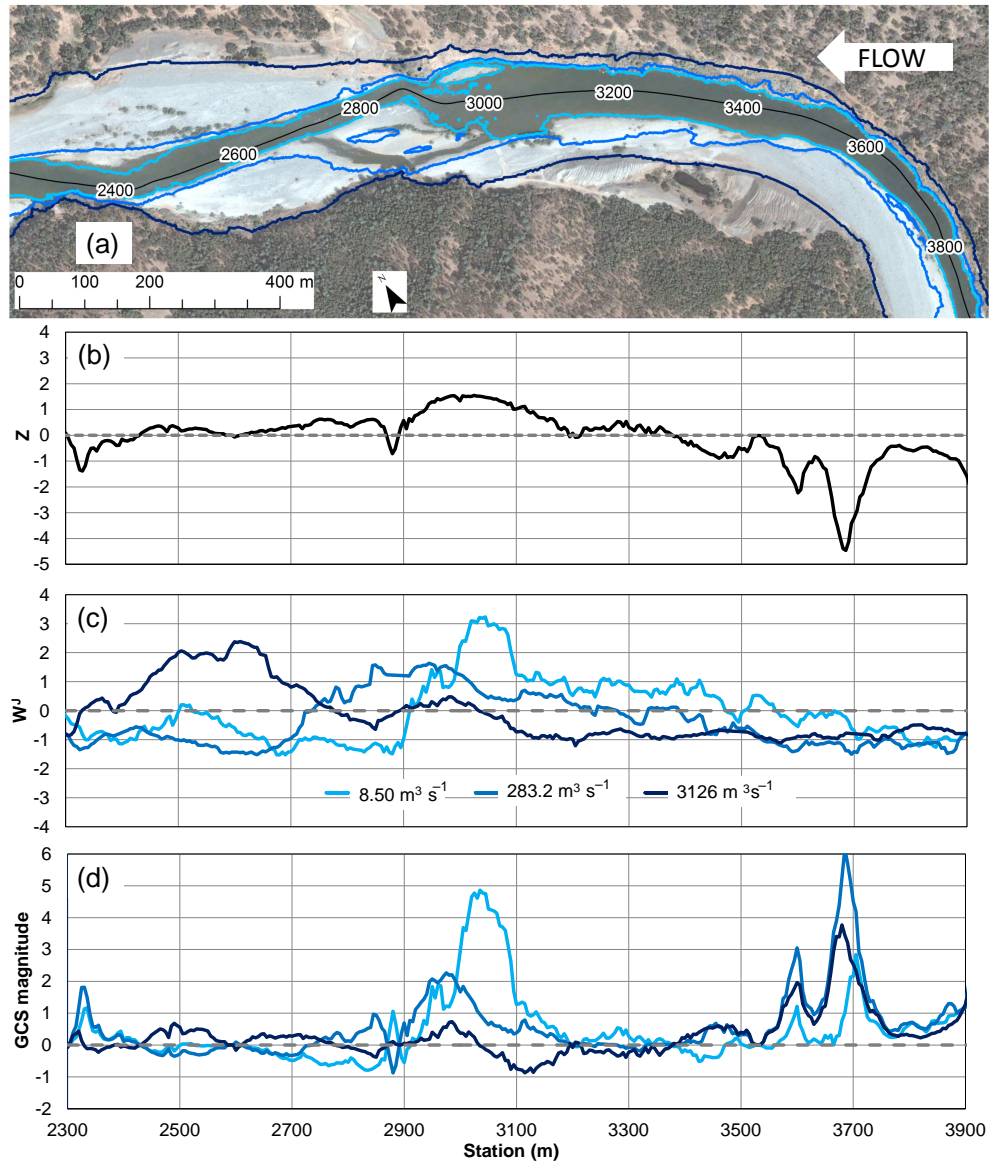


**Figure 5.** Example section at the lower extent of the study area showing inundation extents (a). Below are plots of minimum bed elevation (b), flow widths for 8.50, 283.2, and 3126 m<sup>3</sup> s<sup>-1</sup> (c), and  $C(ZW^j)$  for the same flows. The aerial image is for a flow of 21.29 m<sup>3</sup> s<sup>-1</sup> on 28 September 2006.

## 5.2 Is there a tendency towards positively covarying bed and width oscillations?

The histogram of  $C(ZW^j)$  showed that regardless of discharge, there was a tendency towards positive values (e.g., where both  $Z$  and  $W^j$  covary) and that this changed with stage (Fig. 6a). At least 55 % of the data always had  $C(ZW^j) > 0$ , increasing to 68 % at 283.2 m<sup>3</sup> s<sup>-1</sup> and then slightly declining beyond this flow and stabilizing around 60 % (Fig. 6). There were at most 5 % of values  $< -1$ , with an average and standard deviation of 3 and 2 %, respectively. Contrasting this, values  $> 1$  peaked at 35 % at 141.6 m<sup>3</sup> s<sup>-1</sup> and declined with increasing discharge. So out of the two ex-

tremes, the data exhibited a tendency towards positive values, with negative values  $< -1$  being very rare.

The Mann–Whitney  $U$  test showed interesting flow-dependent aspects of the  $C(ZW^j)$  data sets, where some ranges of flows were significantly different from each other and others were similar (Table 3). For example, the 8.50 m<sup>3</sup> s<sup>-1</sup>  $C(ZW^j)$  had  $p$  values that were all significant at the 95% level for each other flow, indicating differences in their distributions. For flows between 28.32–597.5 m<sup>3</sup> s<sup>-1</sup>, the  $p$  values indicated that the series were statistically similar but not for higher flows. The  $p$  values for 1195, 2390,

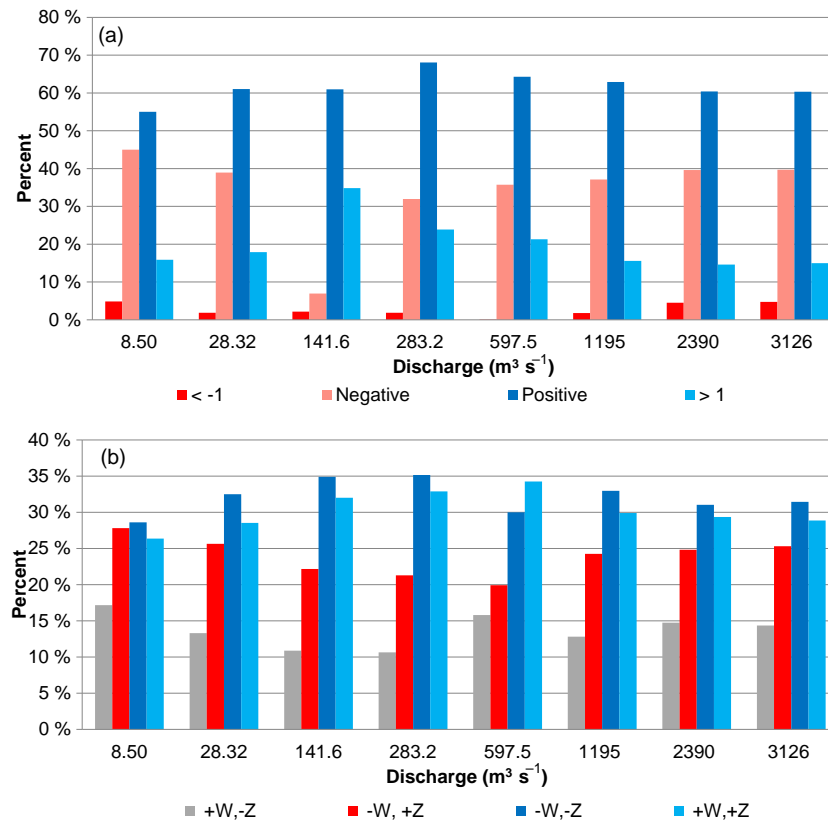


**Figure 6.** Histogram of  $C(ZW^j)$  classified by positive and negative values as well as  $> 1$  and  $< 1$  (a). Also shown is a histogram classified by quadrant (b). The top histogram (a) illustrates the dominance of values  $C(ZW^j) > 0$  regardless of discharge and also illustrates an increasing tendency towards positive values of  $C(ZW^j) > 1$  up until  $141.6 \text{ m}^3 \text{ s}^{-1}$ , after which it declines. The bottom histogram (b) illustrates the distribution of the four quadrant types shown in Fig. 3, with shallow and wide (e.g.,  $+W, +Z$ ) and deep and narrow (e.g.,  $-W, -Z$ ) zones being most dominant at  $283.2 \text{ m}^3 \text{ s}^{-1}$ . Colors represent bin-centered values.

and  $3126 \text{ m}^3 \text{ s}^{-1}$  were statistically similar at the 95 % level but not for lower flows.

The quadrant-based histogram reveals further insight into the distribution of river geometry with flow (Fig. 6b). The average percentage of  $C(ZW^j)$  for each quadrant across all flows was 30 %  $+W, +Z$ ; 14 %  $+W, -Z$ ; 25 %  $-W, +Z$ ; and 31 %  $-W, -Z$ , with standard deviations ranging from 2 to 3 %. Percentages of positive  $C(ZW^j)$  were relatively evenly distributed between  $+W, +Z$  and  $-W, -Z$ , although the latter was slightly more prevalent. The percent of the data in the  $+W, +Z$  quadrant increased from 26 % at  $8.50 \text{ m}^3 \text{ s}^{-1}$ , peaked at 34 % at  $597.5 \text{ m}^3 \text{ s}^{-1}$ , decreased to 30 % at  $1195 \text{ m}^3 \text{ s}^{-1}$  and stabilized near this value for higher flows. Meanwhile, the percent of the data in the  $-W, -Z$  quadrant increased from 29 % at  $8.50 \text{ m}^3 \text{ s}^{-1}$  and peaked at 35 % at  $141.6\text{--}283.2 \text{ m}^3 \text{ s}^{-1}$  flow and then decreased to 30 % at  $597.5 \text{ m}^3 \text{ s}^{-1}$ . After that it increased to 33 % and stabilized at and beyond  $1195 \text{ m}^3 \text{ s}^{-1}$ . Both the  $+W, -Z$  and  $+W, -Z$  quadrants followed a similar but opposite trend, reaching a minimum at  $283.2 \text{ m}^3 \text{ s}^{-1}$ .

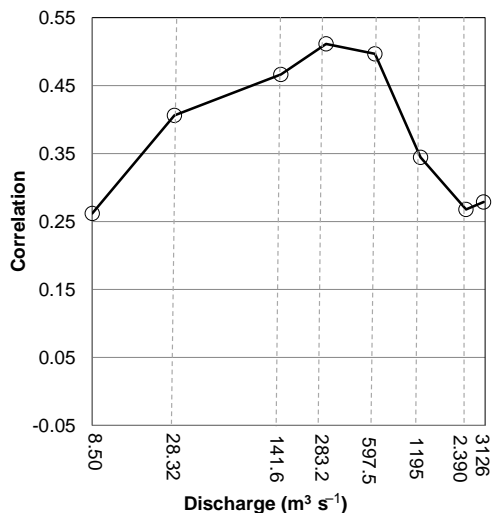
Further insights into the positive nature of  $C(ZW^j)$  can be inferred from bivariate Pearson's correlation coefficients of  $Z$  and  $W^j$  (Fig. 7). Similar to  $C(ZW^j)$  the flow-dependent response was that the correlation between  $Z$  and  $W^j$  increased with flow until  $283.2 \text{ m}^3 \text{ s}^{-1}$  and then subsequently declined. To further reinforce these results, one can also inspect the plot of  $Z, W^j$ , and  $C(ZW^j)$  for  $283.2 \text{ m}^3 \text{ s}^{-1}$ , visually showing the synchronous nature of  $Z$  and  $W^j$  (Fig. 2) The correlations between combinations of  $W^j$  show that each series is significantly correlated to the next highest flow, but there is an interesting flow-dependent pattern (Fig. 8). Correlations between series decrease with increasing flow, reaching a minimum between  $597.5$  and  $1195 \text{ m}^3 \text{ s}^{-1}$  and then increasing again.

### 5.3 Are bed and width oscillations quasiperiodic?

The ACF of  $C(ZW^j)$  also showed similar changes with discharge as the above analyses, with increases in the presence and magnitude of autocorrelation from  $8.50$  to  $597.5 \text{ m}^3 \text{ s}^{-1}$  and then a subsequent decline with increasing flow (Fig. 9a).

**Table 3.** Mann–Whitney  $U$  test  $p$  values amongst all combinations of  $Z$  and  $W^j$ ; bold values are at the 95 % level.

	8.50	28.32	141.6	283.2	597.5	1195	2390	3126
8.50		<b>0.0002</b>	<b>0.0000</b>	<b>0.0000</b>	<b>0.0000</b>	<b>0.0008</b>	<b>0.0498</b>	<b>0.0403</b>
28.32			<b>0.0126</b>	<b>0.0001</b>	<b>0.0262</b>	0.6152	0.0865	0.1009
141.6				0.125	0.7627	<b>0.0015</b>	<b>0.0000</b>	<b>0.0000</b>
283.2					0.0859	<b>0.0000</b>	<b>0.0000</b>	<b>0.0000</b>
597.5						<b>0.0033</b>	<b>0.0000</b>	<b>0.0001</b>
1195							0.2673	0.3129
2390								0.9487
3126								

**Figure 7.** Pearson's correlation coefficient for  $Z$  and  $W^j$  between each flow.

At the lowest discharge there are approximately two broad bands of positive autocorrelation that exceeded both the white noise and AR1 threshold at lag distances of 1400 and 2100 m. At  $28.32 \text{ m}^3 \text{ s}^{-1}$  these three peaks broaden, and the highest correlation was found at lag distance 1400 m, which increased from  $\sim 0.4$  to  $0.7$ . At the bankfull discharge of  $141.6 \text{ m}^3 \text{ s}^{-1}$ , the peak at 1400 m diminishes, while the peak near 2100 m increased in strength (e.g., correlation magnitude). At  $283.2 \text{ m}^3 \text{ s}^{-1}$  there are still peaks near 1400 and 2100 m that exceed both white noise and the AR1 threshold, but two other significant peaks emerge near 700 and 2800 m. Similar statistically significant correlations are found at  $596.5 \text{ m}^3 \text{ s}^{-1}$ , albeit with narrower bands of correlation. The correlation distances at 283.2 and  $596.5 \text{ m}^3 \text{ s}^{-1}$  average  $\sim 700$  m, and this average would have a frequency of approximately  $0.0014 \text{ cycles m}^{-1}$ . Beyond  $596.5 \text{ m}^3 \text{ s}^{-1}$  the ACF diminishes rapidly with no peaks that are statistically significant compared to red noise. Overall, the ACF results show that  $C(ZW^j)$  is quasiperiodic from  $8.50 \text{ m}^3 \text{ s}^{-1}$  to  $141.6\text{--}597.5 \text{ m}^3 \text{ s}^{-1}$ , but then the periodicity decreases in strength as flow increases.

Similar to ACF analysis, PSD analysis showed quasiperiodic components of  $C(ZW^j)$  exhibiting flow-dependent behavior (Fig. 9b). For  $8.50\text{--}283.2 \text{ m}^3 \text{ s}^{-1}$  there is a high power band (e.g.,  $\text{PSD}/\sigma \sim 12\text{--}16$ ) centered on  $0.0014 \text{ cycles m}^{-1}$ , which is confirmed from the ACF analysis above. For  $8.50\text{--}141.6 \text{ m}^3 \text{ s}^{-1}$  there are also smaller magnitude peaks ranging from 3 to 8, spread out over several frequencies. There is also a high magnitude component at the lowest frequency band that emerges at 28.32 and declines by  $283.2 \text{ m}^3 \text{ s}^{-1}$ . These low-frequency components are commonly associated with first-order auto-regressive behavior in the data (Shumway and Stoffer, 2010). At  $597.5 \text{ m}^3 \text{ s}^{-1}$  power is still associated on  $0.0014 \text{ cycles m}^{-1}$ , albeit with a  $\sim 50\%$  reduction in magnitude. Beyond this flow the frequency range and magnitude of statistically significant values decline with discharge. Overall, both ACF and PSD results show that  $C(ZW^j)$  is quasiperiodic from  $8.50$  to  $283.2 \text{ m}^3 \text{ s}^{-1}$  but then decreases in strength as flow increases. Further, the PSD results show that the  $C(ZW^j)$  GCS is flow dependent and multiscale, being characterized by a range of statistically significant frequencies.

## 6 Discussion

### 6.1 Coherent undulations in cobble–gravel bed river topography

The primary result of this study is that in an incising, partly confined, regulated cobble–gravel river whose flow regime is dynamic enough to afford it the capability to rejuvenate its landforms, there was a tendency towards positive  $C(ZW^j)$  and thus covarying  $Z$  and  $W^j$  amongst all flows analyzed. Based on the ACF and PSD analyses, the  $C(ZW^j)$  GCS undulations are quasiperiodic. The results of this study associated channel organization across a range of recurrence interval frequencies within the range of commonly reported channel-forming discharges for western US rivers (e.g., 1.2–2.5 years) as well as substantially larger flows. These conclusions are obviously limited to the study reach, but this should not prohibit discussing possible mechanisms that could lead to these observed patterns, as well as the role of variable flows and incision.

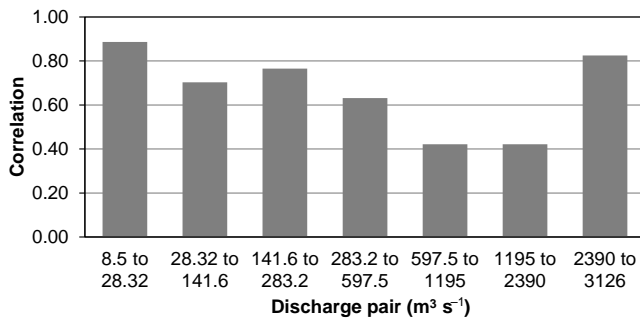


**Figure 8.** Pearson's correlation coefficient for sequential pairs of flow-dependent wetted width series.

Most notably, the test river exhibited a dominance of co-varying values of  $Z$  and  $W^j$  across all flows, being characterized by a quasiperiodic pattern of wide and shallow or narrow and deep cross sections. This supports the idea that alluvial river reaches have a tendency to adopt wide and shallow or narrow and deep cross sections to convey water flow (Huang et al., 2004). Rather than select a single type of cross section to maximize energy dissipation to create a uniform cross section geometry at a single channel-maintaining flow, commonly referred to as bankfull, it appears that alluvial rivers adjust their channel topography to have cross sections that roughly alternate between those that are, on the one hand, wide and shallow and, on the other, narrow and deep (Fig. 6b; Huang et al., 2004), with some locations having a prismatic channel form indicative of normative conditions, particularly in transition zones. Whether this is attributed to minimizing the time rate of potential energy expenditure per unit mass within a reach (Langbein and Leopold, 1962; Yang, 1971; Cherkauer, 1973; Wohl et al., 1999) or channel unit scale mechanisms associated with riffle–pool maintenance (Wilkinson et al. 2004; MacWilliams et al., 2006; Caamano et al., 2009; Thompson, 2010) remains to be determined. Given that extremal hypotheses and riffle–pool maintenance act at different, yet interdependent scales, it is likely that both play an intertwined and inseparable role in channel form. That said, extremal theories are limited to predicting mean channel conditions within a reach (Huang et al., 2014), with no models that can yet fully predict sub-reach-scale alluvial river topography, so we turn our attention to more tractable hydrogeomorphic processes related to the maintenance of riffle and pool topography.

Presumably, the quasi-oscillatory  $C(ZW^j)$  GCS pattern is also linked to flow-dependent patterns of convective acceleration and deceleration zones (Marquis and Roy, 2011; MacVicar and Rennie, 2012), as the length scales of the GCS were aligned with the spacing of erosional and depositional landforms such as bars and pools. This aspect is supported by ACF and PSD results as well as two other studies on the test reach. First, it appears that the quasiperiodicity of the  $C(ZW^j)$  GCS is related to the pool–riffle oscilla-

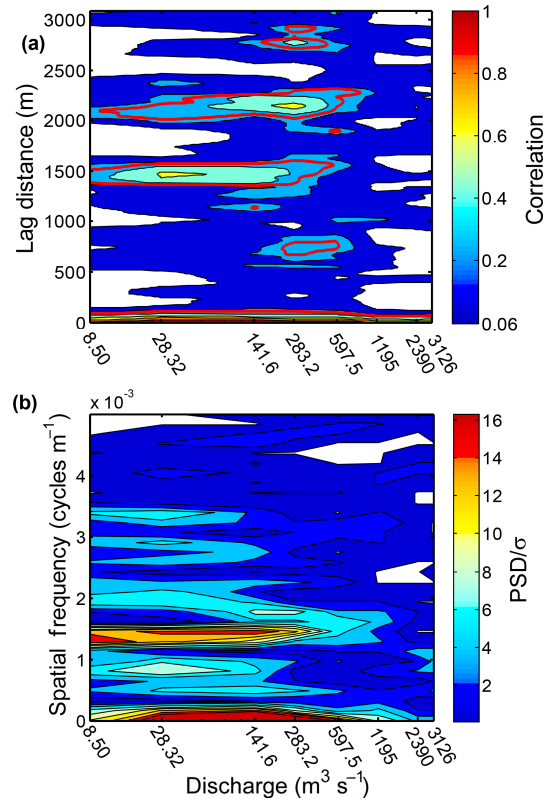


**Figure 9.** Autocorrelation (a) and PSD (b) of  $C(ZW^j)$  with increasing flow. For the ACF plot (a), only values exceeding white noise at the 95 % level are shown and the red contour demarcates the 95 % level for an AR1 process (red noise). For the PSD plot (b) only values exceeding white noise at the 95 % level are shown.

tion in the river corridor. The PSD analysis showed that the dominant frequency of  $C(ZW^j)$  was  $\sim 0.0014 \text{ cycles m}^{-1}$ , which equates to a length scale of  $\sim 700 \text{ m}$  (Fig. 9). Three of the morphologic units (MUs) studied by Wyrick and Pasternack (2014) can be used for context, including pools, riffles, and point bars. In their results for the Timbuctoo Bend reach, pools, riffles, and point bars had an average frequency of 0.0029, 0.0028, and 0.001 cycles  $\text{m}^{-1}$ . Considering that pools and riffles are defined as two end-members of positive  $C(ZW^j)$ , then the frequency of riffles and pools should be twice that of the  $C(ZW^j)$  GCS found herein. That is, a single oscillation of  $C(ZW^j)$  GCS would include both a narrow and deep (e.g., pool) and a wide and shallow (e.g., riffle) cross section geometry, although transitional forms are possible within a cycle, too (Fig. 3). Therefore, it appears that the quasiperiodicity of the  $C(ZW^j)$  GCS is related to the pool–riffle oscillation in the river corridor. This is in agreement with studies based on field investigations and numerical models that relate this observation to quasiperiodic bed and width variations associated with bar–pool topography (Richards, 1976b; Repetto and Tubino, 2001; Carling and Orr, 2002).

Second, Sawyer et al. (2010) showed that stage-dependent flow convergence maintained bed relief by topographically mediated changes in peak velocity and shear stress at the central riffle in a second example (Fig. 5). Interestingly, the flow width series phases relative to bed elevations in accordance with theory (Wilkinson et al., 2004) and field and numerical studies (Brown and Pasternack, 2014). This supports an already reported relationship between the  $C(ZW^j)$  GCS and the process of flow convergence routing (Brown and Pasternack, 2014; Brown et al., 2016).

Lastly, Strom and Pasternack (2016) showed that peak zones of velocity undergo variable changes in their location with discharge, with most velocity reversals occurring after  $597.5 \text{ m}^3 \text{ s}^{-1}$ . In this case the zones of peak velocity patches underwent complex changes from being associated with narrow topographic high points at base flows ( $-W^j, +Z$ ) to topographic low points where flow width is constricted at high flows ( $-W^j, -Z$ ). Overall, the presence of oscillating, on the one hand, wide and shallow and, on the other, narrow and deep cross sections appears to be linked to hydrogeomorphic processes of riffle–pool maintenance.

## 6.2 Hierarchical nesting, variable flows, and the role of incision

This study quantitatively supports the idea that river morphology in partially confined valleys is hierarchically nested with broader exogenic constraints such as the bedrock valley walls, as well as channel-width-scale alluvial controls such as point bars and islands. Our study quantitatively characterized interesting shifts in the amount of correlation amongst flow width series and in the presence of quasiperiodic oscillations in  $C(ZW^j)$  with changes in flow. Each series of  $W^j$  were significantly correlated with the next highest flow, but this was lowest between  $597.5$  and  $1195 \text{ m}^3 \text{ s}^{-1}$ , where the valley walls begin to be engaged (Fig. 7). Further, both the ACF and PSD show that quasiperiodicity in  $C(ZW^j)$  declines after  $597.5 \text{ m}^3 \text{ s}^{-1}$  (Fig. 9). In addition, Strom and Pasternack (2016) showed that reversals in peak velocity occur when flows exceed  $597.5 \text{ m}^3 \text{ s}^{-1}$ . While results show that statistically significant correlations between  $Z$  and  $W^j$  occur for a range of flows, the greatest magnitude is not when the valley walls are inundated, but it is for the  $283.2 \text{ m}^3 \text{ s}^{-1}$  channel and incipient floodplain. Given that correlations were still significant for the flows that inundate the valley walls, this does not refute the role of valley width oscillations in potentially controlling riffle persistence (White et al., 2010) but rather adds new insight to the morphodynamics of rivers incising in partially confined valleys. This suggests that the incision process may be decoupling the organization of the riverbed away from being controlled by the valley walls and instead phased towards reshaping channel topography within the inset bars that are nested within the valley walls. As the riverbed incises further down through knickpoint migration (Carley et al., 2012), this may act to shift zones of high and

low wetted width upstream unless lateral erosion can keep pace.

## 6.3 Broader implications

This study quantified relationships between flow width and minimum bed elevation in a partly confined and incising gravel–cobble-bedded river, as well as for the first time how they change with stage. While study results are currently limited to rivers similar to the study reach, there are several key results of this study that may have broader relevance to river restoration and management.

First, a key result of this study was that channel geometry was organized into covarying  $Z$  and  $W^j$  undulations across all flows analyzed, alternating between, on the one hand, wide and shallow and, on the other, narrow and deep cross sections. This is a very different view from the classical definition of singular and modal bankfull channel geometry often used to guide river and stream restoration (Shields et al., 2003). Instead, our study found that channel geometry at all flows had a relatively even mixture of, on the one hand, wide and shallow and, on the other, narrow and deep cross sections. Studies that deconstruct the complexity of river channel geometry to modal ranges of channel width and depth have always shown scatter, which has mostly been attributed to measurement uncertainty and/or local conditions (Park, 1977; Philips and Harman, 1984; Harman et al., 2008; Surian et al., 2009). Our study suggests that this variability is a fundamental component of alluvial river geometry. While this concept was proposed by Hey and Thorne (1983) over 2 decades ago, few studies have integrated these ideas into river engineering and design (e.g., see Simon et al., 2007). Thus, this study further supports a necessary shift away from designing rivers with modal conditions to designing rivers with quasi-oscillatory and structured variations in channel topography. An example of this is the form–process synthesis of channel topography that experiences flow reversals using GCS theory (Brown et al., 2016)

Second, this study has implications for restoration design and flow reregulation in that a wide array of discharges beyond a single channel-forming flow are presumably needed for alluvial channel maintenance (Parker et al., 2003). Commonly singular values of channel-forming discharge, usually either bankfull or effective discharge, are used in stream and river restoration designs (Shields et al., 2007; Doyle et al., 2007). This study refutes this concept for rivers such as those studied herein, as supported by the results that show gradual changes in channel organization within a band of discharges with recurrence intervals ranging from 1.2 to 5 years, and 4-fold range in absolute discharges. Instead, stream and river restoration practitioners should analyze ranges of flow discharges and the potential topographic features (existing or designed) that could invoke stage-dependent hydrodynamic and geomorphic processes associated with complex, self-maintaining natural rivers.

Third, while the length scales of covarying  $Z$  and  $W^j$  undulations are approximate to the spacing of bars and pools in the study area, they are quite complex and lack explicit cutoffs that illustrate power in a singular frequency band. Thus, river restoration efforts that specify modal values of bedforms may overly simplify the physical structure of rivers with unknown consequences to ecological communities and key functions that are the focus of such efforts. River restoration designs need to mimic the multiscale nature of self-formed topography by incorporating GCS into river engineering (Brown et al., 2014) or somehow ensure that simpler uniscale designs will actually evolve into multiscale ones given available flows and anthropogenic boundary constraints.

Fourth, this study has potential implications for analyzing the effect of flow-dependent responses to topography and physical habitat in river corridors. Valley and channel widths have been shown to be very useful in predicting the intrinsic potential of salmon habitat (Burnett et al., 2007). Further, the role of covarying bed and width undulations in modulating velocity signals and topographic change has implications for the maintenance of geomorphic domains used by aquatic organisms. As one example, consider that adult salmonids use positively covarying zones such as riffles (e.g.,  $+W^j$ ,  $+Z$ ) for spawning and pools (e.g.,  $-W^j$ ,  $-Z$ ) for holding (Bjorn and Reiser, 1991). In the study reach Pasternack et al. (2014) showed that 77% of spawning occurred in riffles and chute morphologic units, which are at or adjacent to areas where  $C(ZW^j) > 1$  (Figs. 4, 5), supporting this idea. The presence and structure of covarying bed and width undulations is also thought to be important indirectly for juvenile salmonids that require shallow and low-velocity zones as refugia during large floods. For example, the expansions that occur at the head of riffles would presumably provide lateral zones of shallow depths and moderate velocities needed for flood refugia. In the absence of positive bed relief, and zones of  $+W$ ,  $+Z$ , flow refugia zones would be hydrologically disconnected from overbank areas, impacting the ability of juvenile salmon to utilize these areas as refugia during floods and potentially leading to population level declines (Nickelson et al., 1992). Future work should better constrain the utility of GCS concepts in assessing aquatic habitat.

Lastly, it is possible that the  $C(ZW^j)$  GCS could be used as a comparative proxy in remote-sensing applications to determine how the topographic structure of rivers changes with flow and how that may also change through time. The zoomed examples of  $C(ZW^j)$  and the detrended river topography highlight how this type of GCS can be used to characterize the topographic influence on wetted width and bed elevation variability in river corridors. The  $C(ZW^j)$  GCS may be used diagnostically to assess riverine structure and hydraulic function in a continuous manner within a river across an array of flows. While not studied herein, prior work (Brown and Pasternack, 2014) showed that the magnitude of  $C(ZW^j)$  can also be related to flow velocity, though lagged effects do oc-

cur. Since the magnitudes can be linked to both unique landforms and flow velocity, they may have utility in assessing topographic and hydraulic controls in river corridors.

Lidar and analytical methods for developing bed topography in rivers have improved considerably (McKean et al., 2009). For example, Gessese et al. (2011) derived an analytical expression for determining bed topography from water surface elevations, which can be obtained from lidar (Magirl et al., 2005). Assuming one has an adequate topographic data set, whether numerical flow modeling is needed to generate wetted width data sets places a considerable constraint on performing this type of analysis. This could potentially be relaxed, especially at flows above bankfull, using a constant water slope approximation for various flow stages. At smaller discharges in rivers, there are typically defects in the water surface elevation, where the bed topography exerts a strong control on bed elevations (e.g., Brown and Pasternack, 2008). However, many studies suggest that on large alluvial rivers, bankfull and flood profiles show that they generally flatten and smoothen once bed forms and large roughness elements such as gravel bars are effectively submerged. In this case, one can then detrend the river corridor and take serial width measurements associated with various heights above the riverbed (Gangodagamage et al., 2007). The height above the river can then be related to estimates of flow discharge and frequency, so that the changed GCS structure can be related to watershed hydrology (Jones, 2006). There is also the obvious option of using paired aerial photography with known river flows by correlating discharge with imagery dates and widths. Future work should establish whether similar conclusions can be reached using field- and model-derived estimates of wetted width as opposed to modeled solutions.

## 7 Conclusions

A key conclusion is that the test river exhibited covarying oscillations of minimum bed elevation and channel top width across all flows analyzed. These covarying oscillations were found to be quasiperiodic at channel-forming flows, scaling with the length scales of pools and riffles. Thus, it appears that alluvial rivers organize their topography to have oscillating, on the one hand, shallow and wide and, on the other, narrow and deep cross section geometry, even despite ongoing incision. Presumably these covarying oscillations are linked to hydrogeomorphic mechanisms associated with alluvial river channel maintenance. As an analytical tool, the GCS concepts here treat the topography of river corridors as system, which is thought of as an essential view in linking physical and ecological processes in river corridors on multiple scales (Fausch et al., 2002; Carbonneau et al., 2012). While much research is needed to validate the utility of these ideas for these broader concepts and applications in ecology

and geomorphology, the idea of GCSs, especially for width and bed elevation, holds promise.

## 8 Data availability

Each  $C(ZW^j)$  data set is available from either author by request.

**The Supplement related to this article is available online at doi:10.5194/esurf-5-1-2017-supplement.**

**Acknowledgements.** Although not directly funded by any source, this study used data and models from studies previously sponsored by Pacific Gas & Electric Company, the US Fish and Wildlife Service Anadromous Fish Restoration Program, Yuba County Water Agency, and the Yuba Accord River Management Team. Co-author Gregory B. Pasternack received support from the USDA National Institute of Food and Agriculture, Hatch project number #CA-D-LAW-7034-H.

Edited by: J. K. Hillier

Reviewed by: C. J. Legleiter, D. Thompson, and J. M. Turowski

## References

- Abu-Aly, T. R., Pasternack, G. B., Wyrick, J. R., Barker, R., Massa, D., and Johnson, T.: Effects of LiDAR-derived, spatially distributed vegetation roughness on two-dimensional hydraulics in a gravel-cobble river at flows of 0.2 to 20 times bankfull, *Geomorphology*, 206, 468–482, doi:10.1016/j.geomorph.2013.10.017, 2014.
- Adler, L. L.: Adjustment of Yuba River, California, to the influx of hydraulic mining debris, 1849–1979, M.A. thesis, Geography Department, University of California, Los Angeles 1980.
- Andrews, E. D.: Effective and bankfull discharges of streams in the Yampa River basin, Colorado and Wyoming, *J. Hydrol.*, 46, 311–330, 1980.
- Bjorn, T. C. and Reiser, D. W.: Habitat Requirements of Salmonids in Streams, in: Influences of Forest and Rangeland Management on Salmonid Fishes and Their Habitats, edited by: Meehan, W. R., Special Publication 19, American Fisheries Society, Bethesda, MD, 83–138, 1991.
- Brown, R. A.: The Analysis and Synthesis of River Topography (Doctoral Dissertation) University Of California, Davis, 187 pp., 2014.
- Brown, R. A. and Pasternack, G. B.: Engineered channel controls limiting spawning habitat rehabilitation success on regulated gravel-bed rivers, *Geomorphology*, 97, 631–654, 2008.
- Brown, R. A. and Pasternack, G. B.: Hydrologic and Topographic Variability Modulate Channel Change in Mountain Rivers, *J. Hydrol.*, 510, 551–564, doi:10.1016/j.jhydrol.2013.12.048, 2014.
- Brown, R. A., Pasternack, G. B., and Wallender, W. W.: Synthetic River Valleys: Creating Prescribed Topography for Form-Process Inquiry and River Rehabilitation Design, *Geomorphology*, 214, 929–942, 2014.
- Brown, R. A., Pasternack, G. B., and Lin, T.: The topographic design of river channels for form-process linkages, *Environ. Manage.*, 57, 929–942, 2016.
- Burnett, K. M., Reeves, G. H., Miller, D. J., Clarke, S., Vance-Borland, K., and Christiansen, K.: Distribution Of Salmon-Habitat Potential Relative To Landscape Characteristics And Implications For Conservation, *Ecol. Appl.*, 17, 66–80, 2007.
- Caamaño, D., Goodwin, P., and Buffington, J. M.: Unifying criterion for the velocity reversal hypothesis in gravel-bed rivers, *J. Hydraul. Engin.*, 135, 66–70, 2009.
- Carboneau, P., Fonstad, M. A., Marcus, W. A., and Dugdale, S. J.: Making riverscapes real, *Geomorphology*, 137, 74–86, doi:10.1016/j.geomorph.2010.09.030, 2012.
- Carley, J. K., Pasternack, G. B., Wyrick, J. R., Barker, J. R., Bratovich, P. M., Massa, D., Reedy, G., and Johnson, T. R.: Significant decadal channel change 58–67 years post-dam accounting for uncertainty in topographic change detection between contour maps and point cloud models, *Geomorphology*, 179, 71–88, doi:10.1016/j.geomorph.2012.08.001, 2012.
- Carling, P. A. and Orr, H. G.: Morphology of riffle-pool sequences in the River Severn, England, *Earth Surf. Proc. Land.*, 2, 369–384, 2000.
- Carter, G., Knapp, C., and Nuttall, A.: Estimation of the magnitude-squared coherence function via overlapped fast Fourier transform processing, *IEEE T. Acoust. Speech.*, 21, 337–344, doi:10.1109/TAU.1973.1162496, 1973.
- Cherkauer, D. S.: Minimization of power expenditure in a riffle-pool alluvial channel, *Water Resour. Res.*, 9, 1613–1628, 1973.
- Church, M.: Multiple scales in rivers, in: *Developments in Earth Surface Processes*, edited by: Habersack, H., Piégay, H., and Rinaldi, M., Elsevier, 2007, 11, 3–28, ISSN 0928-2025, ISBN 9780444528612, 2006.
- Cienciala, P. and Pasternack, G. B.: Floodplain Inundation Response to Climate, Valley Form, and Flow Regulation on a Gravel-Bed River in a Mediterranean-Climate Region, *Geomorphology*, in press, 2016.
- Colombini, M., Seminara, G., and Tubino, M.: Finite-amplitude alternate bars, *J. Fluid Mechan.*, 181, 213–232, doi:10.1017/S0022112087002064, 1987.
- Cox, N. J.: On the estimation of spatial autocorrelation in geomorphology, *Earth Surf. Proc. Land.*, 8, 89–93, doi:10.1002/esp.3290080109, 1983.
- Davis, W. M.: *The Geographical Cycle*, Chapter 13, *Geographical Essays*, Ginn and Co., New York, 1909.
- DeAlmeida, G. A. M. and Rodriguez, J. F.: Spontaneous formation and degradation of pool-riffle morphology and sediment sorting using a simple fractional transport model, *Geophys. Res. Lett.*, 39, L06407, doi:10.1029/2012GL051059, 2012.
- Dolan, R., Howard, A., and Trimble, D.: Structural control of the rapids and pools of the Colorado River in the Grand Canyon, *Science*, 10, 629–631, doi:10.1126/science.202.4368.629, 1978.
- Doyle, M. W., Shields, D., Boyd, K. F., Skidmore, P. B., and Dominick, D.: Channel-Forming Discharge Selection in River Restoration Design, *J. Hydraul. Engin.*, 133, 831–837, 2007.
- Escobar-Arias, M. I. and Pasternack, G. B.: Differences in River Ecological Functions Due to Rapid Channel Alteration Processes in Two California Rivers Using the Functional Flows Model, Part 2 – Model Applications, *River Res. Appl.*, 27, 1–22, doi:10.1002/rra.1335, 2011.

- Frissell, C. A., Liss, W. J., Warren, C. E., and Hurley, M. D.: A hierarchical framework for stream habitat classification: Viewing streams in a watershed context, *Environ. Manage.*, 10, 199–214, 1986.
- Gangodagamage, C., Barnes, E., and Fofoula Georgiou, E.: Scaling in river corridor widths depicts organization in valley morphology, *Geomorphology*, 91, 198–215, doi:10.1016/j.geomorph.2007.04.014, 2007.
- Gessese, A. F., Sellier, M., Van Houten, E., and Smart, G.: Reconstruction of river bed topography from free surface data using a direct numerical approach in one-dimensional shallow water flow, *Inverse Probl.*, 27, 12 pp., 2011.
- Ghoshal, S., James, L. A., Singer, M. B., and Aalto, R.: Channel and Floodplain Change Analysis over a 100-Year Period: Lower Yuba River, California, *Remote Sens.*, 2, 1797–1825, 2010.
- Gilbert, G. K.: Hydraulic-mining debris in the Sierra Nevada, United States Geological Survey Professional Paper, 105, 154 pp., 1917.
- Guinn, J. M.: Exceptional years: a history of California floods and drought, *Historical Society of Southern California*, 1, 33–39, 1890.
- Harman, C., Stewardson, M., and DeRose, R.: Variability and uncertainty in reach bankfull hydraulic geometry, *J. Hydrol.*, 351, 13–25, doi:10.1016/j.jhydrol.2007.11.015, 2008.
- Harrison, L. R. and Keller, E. A.: Modeling forced pool–riffle hydraulics in a boulder-bed stream, southern California, *Geomorphology*, 83, 232–248, doi:10.1016/j.geomorph.2006.02.024, 2007.
- Hernandez, G.: Time series, periodograms, and significance, *J. Geophys. Res.*, 104, 10355–10368, doi:10.1029/1999JA900026, 1999.
- Hey, R. D. and Thorne, C. R.: Stable channels with mobile gravel beds, *J. Hydraul. Engin.*, 112, 671–689, 1986.
- Huang, H. Q., Chang, H. H., and Nanson, G. C.: Minimum energy as the general form of critical flow and maximum flow efficiency and for explaining variations in river channel pattern, *Water Resour. Res.*, 40, W04502, doi:10.1029/2003WR002539, 2004.
- Huang, H. Q., Deng, C., Nanson, G. C., Fan, B., Liu, X., Liu, T., and Ma, Y.: A test of equilibrium theory and a demonstration of its practical application for predicting the morphodynamics of the Yangtze River, *Earth Surf. Proc. Land.*, 39, 669–675, 2014.
- Jackson, J. R., Pasternack, G. B., and Wyrick, J. R.: Substrate of the Lower Yuba River. Prepared for the Yuba Accord River Management Team, University of California, Davis, CA, 61 pp., 2013.
- James, L. A., Singer, M. B., and Ghoshal, S.: Historical channel changes in the lower Yuba and Feather Rivers, California: Long-term effects of contrasting river-management strategies, *Geol. Soc. Am. Spec. Papers*, 451, 57–81, doi:10.1130/2009.245104, 2009.
- Keller, E.: Areal Sorting of Bed-Load Material: The Hypothesis of Velocity Reversal, *Geol. Soc. Am. Bull.*, 82, 753–756, 1971.
- Keller, E. A. and Melhorn, W. N.: Rhythmic spacing and origin of pools and riffles, *GSA Bull.*, 89, 723–730, 1978.
- Knighton, A.: Models of stream bed topography at the reach scale, *J. Hydrol.*, 60, 105–121, 1983.
- Lisle, T.: A Sorting Mechanism For A Riffle-Pool Sequence, *Geol. Soc. Am. Bull.*, Part 11, 90, 1142–1157, 1979.
- Leopold, L. B. and Maddock, T.: The Hydraulic Geometry of Stream Channels and Some Physiographic Implications, *Geological Survey Professional Paper 252*, United States Geological Survey, Washington, DC, 1953.
- Leopold, L. B. and Langbein, W. B.: The Concept of Entropy in Landscape Evolution, US Geological Survey Professional Paper 500-A, 20 pp., 1962.
- MacWilliams Jr, M. L., Wheaton, J. M., Pasternack, G. B., Street, R. L., and Kitanidis, P. K.: Flow convergence routing hypothesis for pool–riffle maintenance in alluvial rivers, *Water Resour. Res.*, 42, W10427, doi:10.1029/2005WR004391, 2006.
- MacVicar, B. J. and Rennie, C. D.: Flow and turbulence redistribution in a straight artificial pool, *Water Resour. Res.*, 48, W02503, doi:10.1029/2010WR009374, 2012.
- Madej, M. A.: Development of channel organization and roughness following sediment pulses in single-thread, gravel bed rivers, *Water Resour. Res.*, 37, 2259–2272, doi:10.1029/2001WR000229, 2001.
- Magirl, C. S., Webb, R. H., and Griffiths, P. G.: Changes in the water surface profile of the Colorado River in Grand Canyon, Arizona, between 1923 and 2000, *Water Resour. Res.*, 41, W05021, doi:10.1029/2003WR002519, 2005.
- Marquis, G. A. and Roy, A. G.: Bridging the gap between turbulence and larger scales of flow motions in rivers, *Earth Surf. Proc. Land.*, 36, 563–568, doi:10.1002/esp.2131, 2011.
- McKean, J. A., Isaac, D. J., and Wright, C. W.: Geomorphic controls on salmon nesting patterns described by a new, narrow-beam terrestrial–aquatic lidar, *Front. Ecol. Environ.*, 6, 125–130, doi:10.1890/070109, 2008.
- McKean, J., Nagel, D., Tonina, D., Bailey, P., Wright, C. W., Bohn, C., and Nayegandhi, A.: Remote sensing of channels and riparian zones with a narrow-beam aquatic–terrestrial lidar, *Remote Sens.*, 1, 1065–1096, doi:10.3390/rs1041065, 2009.
- Melton, M. A.: Methods for measuring the effect of environmental factors on channel properties, *J. Geophys. Res.*, 67, 1485–1490, doi:10.1029/JZ067i004p01485, 1962.
- Milan, D. J., Heritage, G. L., Large, A. R. G., and Charlton, M. E.: Stage dependent variability in tractive force distribution through a riffle-pool sequence, *Catena*, 44, 85–109, 2001.
- Milne, J. A.: Bed-material size and the riffle-pool sequence, *Sedimentology*, 29, 267–278, doi:10.1111/j.1365-3091.1982.tb01723.x, 1982.
- Nelson, P. A., Brew, A. K., and Morgan, J. A.: Morphodynamic response of a variable-width channel to changes in sediment supply, *Water Resour. Res.*, 51, 5717–5734, doi:10.1002/2014WR016806, 2015.
- Newland, D. E.: An introduction to random vibrations, spectral and wavelet analysis, Dover Publications, 1993.
- Nickelson, T. A., Rodgers, J., Johnson, S. L., and Solazzi, M. F.: Seasonal Changes in Habitat Use by Juvenile Coho Salmon (*Oncorhynchus kisutch*) in Oregon Coastal Streams, *Can. J. Fish. Aquat. Sci.*, 49, 783–789, doi:10.1139/f92-088, 1992.
- Nolan, K. M., Lisle, T. E., and Kelsey, H. M.: Bankfull discharge and sediment transport in northwestern California, in: Erosion and Sedimentation in the Pacific Rim (Proceedings of the Corvallis Symposium, August 1987), edited by: Beschta, R., Blinn, T., Grant, G. E., Swanson, F. J., and Ice, G. G., *Int. Assoc. Hydrol. Sci. Pub.*, 165, 439–449, 1987.
- Park, C. C.: World-wide variations in hydraulic geometry exponents of stream channels: An analysis and some observations, *J. Hydrol.*, 33, 133–146, 1977.

- Parker, G., Toro-Escobar, C. M., Ramey, M., and Beck, S.: The effect of floodwater extraction on the morphology of mountain streams, *J. Hydraul. Engin.*, 129, 885–895, 2003.
- Pasternack, G. B. and Wyrick, J. R.: Flood-driven topographic changes in a gravel-cobble river over segment, reach, and unit scales, *Earth Surf. Proc. Land.*, in press, 2016.
- Pasternack, G. B., Tu, D., and Wyrick, J. R.: Chinook adult spawning physical habitat of the lower Yuba River. Prepared for the Yuba Accord River Management Team, University of California, Davis, CA, 154 pp., 2014.
- Phillips, P. J. and Harlin, J. M.: Spatial dependency of hydraulic geometry exponents in a subalpine stream, *J. Hydrol.*, 71, 277–283, 1984.
- Pike, R. J., Evans, I., and Hengl, T.: *Geomorphometry: A Brief Guide*, in: *Geomorphometry – Concepts, Software, Applications*, edited by: Hengl, T. and Reuter, H. I., Series Developments in Soil Science, Elsevier, 33, 3–33, ISBN 978-0-12-374345-9, 2008.
- Rayburg, S. C. and Neave, M.: Assessing morphologic complexity and diversity in river systems using three-dimensional asymmetry indices for bed elements, bedforms and bar units, *River Res. Appl.*, 24, 1343–1361, doi:10.1002/rra.1096, 2008.
- Rendell, H. and Alexander, D.: Note on some spatial and temporal variations in ephemeral channel form, *Geol. Soc. Am. Bull.*, 9, 761–772, 1979.
- Repetto, R. and Tubino, M.: Topographic Expressions of Bars in Channels with Variable Width, *Phys. Chem. Earth B*, 26, 71–76, 2001.
- Richards, K. S.: The morphology of riffle-pool sequences, *Earth Surf. Proc.*, 1, 71–88, doi:10.1002/esp.3290010108, 1976a.
- Richards, K. S.: Channel width and the riffle-pool sequence, *Geol. Soc. Am. Bull.*, 87, 883–890, 1976b.
- Richards, K. S.: Stochastic processes in one dimension: An introduction, *Concepts and Techniques In Modern Geography*, 23, 30 pp., 1979.
- Richter, B. D., Braun, D. P., Mendelson, M. A., and Master, L. L.: Threats to Imperiled Freshwater Fauna, *Conserv. Biol.*, 11, 1081–1093, 1997.
- Rosgen, D.: *Applied River Morphology (Wildland Hydrology, Pagosa Springs, Colorado)*, Wildland Hydrology, Pagosa Springs, CO, 1996.
- Salas, J. D.: *Applied modeling of hydrologic time series. Applied modeling of hydrologic time series*, Water Resources Publications, Littleton, Colorado, 1980.
- Sawyer, A. M., Pasternack, G. B., Moir, H. J., and Fulton, A. A.: Riffle-pool maintenance and flow convergence routing confirmed on a large gravel bed river, *Geomorphology*, 114, 143–160, 2010.
- Schumm, S. A.: Fluvial geomorphology: channel adjustment and river metamorphosis, in: *River Mechanics*, edited by: Shen, H. W., Fort Collins, CO, 1–22, 1971.
- Shields, D., Copeland, R., Klingeman, P., Doyle, M., and Simon, A.: Design for Stream Restoration, *J. Hydraul. Engin.*, 129, 575–584, doi:10.1061/(ASCE)0733-9429(2003)129:8(575), 2003.
- Shumway, R. H. and Stoffer, D. S.: *Time series analysis and its applications: with R examples*, Time series analysis and its applications: with R examples, 505 pp., Springer US, 2010.
- Simon, A. M., Doyle, M., Kondolf, M., Shields, F. D., Rhoads, B., and McPhillips, M.: Critical Evaluation of How the Rosgen Classification and Associated “Natural Channel Design” Methods Fail to Integrate and Quantify Fluvial Processes and Channel Response, *J. Am. Water Resour. Assoc.*, 43, 1117–1131, doi:10.1111/j.1752-1688.2007.00091.x, 2007.
- Strom, M. A., Pasternack, G. B., and Wyrick, J. R.: Reenvisioning velocity reversal as a diversity of hydraulic patch behaviors, *Hydrol. Proc.*, 723–737, doi:10.1002/hyp.10797, 2016.
- Surian, N., Mao, L., Giacomini, M., and Ziliani, L.: Morphological effects of different channel-forming discharges in a gravel-bed river, *Earth Surf. Proc. Land.*, 34, 1093–1107, doi:10.1002/esp.1798, 2009.
- Thompson, D. M.: The velocity-reversal hypothesis revisited, *Prog. Phys. Geogr.*, 35, 123–132, doi:10.1177/0309133310369921, 2010.
- Thomson, J. R., Taylor, M. P., Fryirs, K. A., and Brierley, G. J.: A geomorphological framework for river characterization and habitat assessment, *Aquat. Conserv.*, 11, 373–389, 2001.
- Thornbury, W. D.: *Principles of geomorphology*, John Wiley, New York, 1954.
- Trauth, M. H., Gebbers, R., Marwan, N., and Sillmann, E.: *MATLAB recipes for earth sciences*, Springer, 2006.
- White, J. Q., Pasternack, G. B., and Moir, H. J.: Valley width variation influences riffle-pool location and persistence on a rapidly incising gravel-bed river, *Geomorphology*, 121, 206–221, doi:10.1016/j.geomorph.2010.04.012, 2010.
- Wolman, M. G. and Gerson, R.: Relative Scales of Time and Effectiveness of Climate in Watershed Geomorphology, *Earth Surf. Proc. Land.*, 3, 189–208, 1978.
- Wilkinson, S. N., Keller, R. J., and Rutherford, I. D.: Phase-shifts in shear stress as an explanation for the maintenance of pool-riffle sequences, *Earth Surf. Proc. Land.*, 29, 737–753, doi:10.1002/esp.1066, 2004.
- Williams, G. P.: Bank-full discharge of rivers, *Water Resour. Res.*, 14, 1141–1154, doi:10.1029/WR014i006p01141, 1978.
- Wohl, E. E., Thompson, D. M., and Miller, A. J.: Canyons with undulating walls, *Geol. Soc. Am. Bull.*, 111, 949–959, 1999.
- Wolman, M. G. and Gerson, R.: Relative scales of time and effectiveness of climate in watershed geomorphology, *Earth Surf. Proc. Land.*, 3, 189–208, doi:10.1002/esp.3290030207, 1978.
- Wyrick, J. R. and Pasternack, G. B.: Landforms of the lower Yuba River, University of California, Davis, 2012.
- Wyrick, J. R. and Pasternack, G. B.: Geospatial organization of fluvial landforms in a gravel-cobble river: Beyond the riffle-pool couplet, *Geomorphology*, 213, 48–65, doi:10.1016/j.geomorph.2013.12.040, 2014.
- Wyrick, J. R. and Pasternack, G. B.: Revealing the natural complexity of topographic change processes through repeat surveys and decision-tree classification, *Earth Surf. Proc. Land.*, 311–322, doi:10.1002/esp.3854, 2015.
- Yalin, M. S.: *Mechanics of sediment transport*, Elsevier, 1977.
- Yang, C. T.: Potential Energy and Stream Morphology, *Water Resour. Res.*, 7, 311–322, doi:10.1029/WR007i002p00311, 1971.
- Yu, B. and Wolman, M. G.: Some dynamic aspects of river geometry, *Water Resour. Res.*, 23, 501–509, doi:10.1029/WR023i003p00501, 1987.